ANTIFERROMAGNETISM IN $CsMnF_3$

ANTIFERROMAGNETISM IN $CsMnF_3$

By

DJAMSHID KHATAMIAN, B.Sc.,M.Sc.

A Thesis

Submitted to the Faculty of Graduate Studies

in Partial Fulfilment of the Requirements

for the Degree

Doctor of Philosophy

McMaster University

September 1976

DOCTOR OF PHILOSOPHY (1976)
(Physics)

McMASTER UNIVERSITY
Hamilton, Ontario

TITLE: Antiferromagnetism in $CsMnF_3$

AUTHOR: Djamshid Khatamian, B.Sc. (University of Azarabadegan)

M.Sc. (Eastern Michigan University)

SUPERVISOR: Professor M. F. Collins

NUMBER OF PAGES: x, 96

ABSTRACT

Two of the magnetic properties of antiferromagnet, $CsMnF_3$, were studied by thermal neutron scattering techniques.

Spin wave dispersion curves, along the two high symmetry directions (00ξ) and $(\xi 00)$, were determined and were satisfactorily fitted to a theoretical model with two nearest neighbour exchange constants, J_{12} = 0.134±.003 THz and J_{23} = 0.094±.0105 THz, and one second nearest neighbour exchange constant, J_{35} = - 0.0138±.003 THz. The spin wave properties can be described in terms of an effective anisotropy field of -2700±900 Oe along the crystal c axis. This field constrains the spins to the basal plane of the crystal. The calculations show that magnetic dipole-dipole interactions, alone, provide enough anisotropy to account for the observed results.

The sublattice magnetization, over the temperature range of 6.8 K to 72.2 K, was measured. This shows a critical phase transition with a critical exponent β given by β = 0.317±.009.

ACKNOWLEDGEMENT

This work was begun at the suggestion of Professor M.F. Collins and was carried out under his direction. I feel highly indebted to Professor Collins for his keen interest and guidance throughout the course of this research.

I would like to thank Professor B.N. Brockhouse, F.R.S., for the use of his neutron spectrometers at McMaster and at Chalk River Nuclear Laboratories.

To my colleagues at McMaster University: Mr. R. Boire, Mr. J. Couper, Mr. D. Hodgson, Dr. A. Larose, Mr. J. Oyedele and Mr. C. Papanastasopoulos go my sincere thanks for providing a congenial atmosphere, for many valuable discussions and for assistance throughout the course of this work.

This work was supported by the National Research Council of Canada, the McMaster University Physics Department, by a McMaster University Benefactors Scholarship and by the provision of research facilities by the Atomic Energy of Canada Ltd., Chalk River, Ontario.

I am sincerely grateful to Mrs. H. Kennelly, who patiently and accurately typed this manuscript.

Finally, I would like to thank my wife, Mahvash, for her patience, optimism and encouragement when it was needed most.

THIS THESIS IS DEDICATED TO MY PARENTS

TABLE OF CONTENTS

LIST OF ILLUSTRATIONS

LIST OF TABLES

Every created thing in the whole universe is but a door leading into His knowledge, a sign of His sovereignty, a revelation of His names, a symbol of His majesty, a token of His power, a means of admittance into His straight Path.

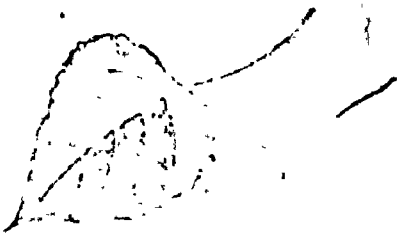

Bahá'u'lláh

CHAPTER I

INTRODUCTION

This thesis describes experiments to measure two of the magnetic properties of the antiferromagnet $CsMnF_3$. The first experiment concerns the determination of the frequency of excitations of the magnetic system at low temperature; these excitations are known as spin waves and from measurements of their frequency we can determine the nature of the interactions between the magnetic moments in the atoms. The second experiment measures the magnitude of the aligned moments as a function of temperature; the moments are aligned below a temperature known as the Néel temperature and the transition from the aligned to non-aligned state is of a type known as a critical phase transition. The information provided by the experiment contributes to knowledge of critical phase transitions.

I-1 Magnetism:

In the first part of this section we shall talk briefly about different types of magnetic-order and in the second part the interactions which bring about such magnetic order will be discussed. A more complete historical introduction to magnetism can be found in the books, "The theory of magnetism"

by Mattis (1965) and "Magnetism and matter" by Stoner (1934).

a - Magnetic order: Many crystals have an ordered magnetic structure. This means that, in the absence of an external magnetic field, the mean magnetic moment of at least one of the atoms in each unit cell of the crystal is non-zero.

In the simplest type of magnetically-ordered crystals, that is ferromagnets such as Fe, Ni, Co and Gd, the mean magnetic moments of all the atoms have the same orientation provided that the temperature does not exceed a critical value known as the Curie temperature. This alignment of the moments gives rise to spontaneous magnetic moments on a macroscopic scale, even in the absence of an external magnetic field.

Almost all salts of the later 3d transition metals (Mn, Fe, Co, Ni) are found to be antiferromagnets. Antiferromagnets are materials where the moments of the magnetic atoms are aligned, but the alignment is such that, for every atom on a particular crystal site, there is another atom on an equivalent site with an antiparallel alignment of its moment. Experiments have shown that such situations occur very commonly in the halides, chalcogenides, pnictides, sulphates, carbonates, nitrates and other salts of the transition metals. To account for the antiferromagnetism, an antiferromagnetic crystal must consist of a set of sublattices (called magnetic sublattices), each of which has a non zero mean magnetic moment, but the sum of the mean moments of the sublattices

[illegible] of [illegible] if the

ture of the antiferromagnet is less than a critical temperature known as the Néel temperature.

Another class of magnetically ordered materials are the ferrimagnets. These consist of a number of magnetic sublattices whose magnetic moments are uncompensated (in contrast to antiferromagnets) and so exhibit a spontaneous magnetic moment. Examples of this type are compounds of transition metals such as the ferrites Fe_3O_4, $MnFe_2O_4$, $CoFe_2O_4$ etc. There are more complicated magnetic orderings such as, helical, canted and modulated structures, but we shall not discuss them in this thesis.

b - Exchange and superexchange interactions: The magnetic order in ferromagnets and antiferromagnets is the result of correlation between the directions of the electron spins on individual atoms. This correlation is in turn due to the fact that the space symmetry of the wave function depends on the magnitude of the resultant spin of the system of electrons. This dependence is a consequence of the principle of indistinguishability of identical particles and is responsible for the fact that the energy of the system depends on the magnitude of its resultant spin, since different values of the energy of the system in general correspond to wave functions with different space symmetry.

It is important to note that these effects occur even if the Hamiltonian for the system does not contain terms

describing magnetic, that is relativistic, interactions between the electrons. Thus we are discussing a purely quantum mechanical effect which results from the fact that electrons obey Fermi-Dirac statistics. This effect is called the exchange effect, and the dependence of the energy of the system on the magnitude of its resultant spin is referred to as being due to the exchange interaction.

It was Heisenberg (1926) who pointed out that ordinary electrostatic interactions among electrons, together with the Pauli exclusion principle, could lead to an exchange interaction which strongly coupled the electron spins. For an assembly of local orbitals Dirac (1929) showed that the exchange interaction may be written as

$$H_{ex} = - \sum_{m,n} J_{mn} \underline{S}_m \cdot \underline{S}_n \qquad (I\text{-}1)$$

where J_{mn} is the exchange integral, $\underline{S}_m$ is the spin of atom m and $\underline{S}_n$ the spin of atom n. Clearly for $J_{mn} > 0$ the lowest state of such an interaction is that in which all spins are parallel, or ferromagnetic. J_{mn} depends upon the distance between atoms m and n, and falls off rapidly with increasing distance, because there is no significant overlap of orbitals beyond near neighbor atoms.

Néel (1932) expressed the idea that interactions with negative sign (i.e. $J_{mn} < 0$) can lead to antiferromagnetism, in which different sublattices of spins in a crystal can align

themselves antiparallel. Most insulating magnetic materials are observed to be antiferromagnetic at low temperatures. In 1934 Kramers proposed that the magnetic cations have wave functions which are strongly admixed with anion wave functions. This makes it possible for cations to couple indirectly. Because the magnetic cations are separated by at least one anion, Kramers called this type of exchange "superexchange". Perturbation theory gives an effective exchange from this mechanism, though it can be shown that the theory is poorly convergent. Anderson (1959) developed a method which overcomes the convergence problem. In this approach he first constructs the wave functions of magnetic ions surrounded by the various diamagnetic anions, exclusive of the exchange effects of the other magnetic ions, and then lets the magnetic ions interact. He showed that the admixture of p wave functions into the magnetic wave function is the primary mechanism for superexchange. Thus superexchange is a direct result of covalent binding effects in magnetic crystals.

I-2 Spin Waves or Magnons:

The so-called Heisenberg Hamiltonian given by equation (I-1) has been employed for several decades, both as a tool for a large number of studies in theoretical physics and as an extremely powerful model for the interpretation of a wide variety of experimental properties of insulating magnetic crystals. It is found to account successfully for many properties of a wide variety of materials.

With the Heisenberg Hamiltonian as the basic ingredient in the magnetic Hamiltonian, F. Bloch (1930) and J. C. Slater (1930) showed that spin waves were the elementary excitations from the ordered ground state at low temperatures.

There are some similarities between the elementary excitations in a magnetic material and those of an elastic solid. In the latter, we know that if an atom is displaced from its equilibrium position, it will oscillate with the motion and frequencies associated with the harmonic oscillators, or normal modes of the crystal. The effect of quantum mechanics on this motion is to quantize the energies of the normal modes, with the resulting quanta known as phonons. The analogous normal modes, in materials with an ordered magnetic structure, are the spin waves. When the quantum mechanical nature of spins is taken into account, these are also quantized with the quanta of energy known as magnons.

There are excellent reviews and books available on spin waves, including the books, "The theory of magnetism" by Mattis (1965), "Spin waves" by Akheizer, Bar'yakhtar and Peletminskii (1968), and "Elements of theoretical magnetism" by Krupicka (1968), and the reviews by Hennion (1972), Keffer (1966) and Kranendonk and Van Vleck (1958).

We shall develop spin wave theory in Chapter II and apply it to $CsMnF_3$, which is an antiferromagnet with six sublattices per unit cell. Chapter III will deal with the ways of measuring spin wave energies by means of thermal neutron

spectroscopy. In Chapter IV we shall present the results of neutron scattering experiments in $CsMnF_3$ and shall fit them to the theoretical model.

I-3 Critical Phase Transitions:

Phase transitions are one of the striking aspects of the macroscopic physical world. In many cases the various phases of matter seem quite dissimilar and separate, and transitions between them are abrupt. Nevertheless, by varying the temperature or other thermodynamic parameters, two distinct phases can frequently be made more and more similar in their properties until, finally, at a certain critical point, all differences vanish. Beyond this point only one homogeneous equilibrium phase exists and all changes are continuous and smooth. The most familiar example of such a critical point is that which terminates the coexistence curve of a liquid and its vapour at a characteristic temperature, pressure and density, T_c, P_c and ρ_c. The Curie point of a ferromagnetic crystal is where the spontaneous magnetization goes continuously to zero and the Néel point is where the alternating spin order of an antiferromagnet disappear.

In a formal way those transitions in which one or more first derivatives of the relevant thermodynamic potentials change discontinuously as a function of their variables may be called "first-order phase transitions". For a fluid it is appropriate to consider the Gibbs free energy G as a function

of P and T; the specific volume $v = (\frac{\partial G}{\partial P})_T$ and the entropy $s = -(\frac{\partial G}{\partial T})_P$ are discontinuous across the vapour pressure curve. In a ferromagnet the equilibrium magnetization $M = -(\frac{\partial F}{\partial H})_T$, where F is the Helmholtz free energy and H the magnetic field, changes abruptly as the field passes through zero when T is less than T_c.

In contrast, transitions in which the first derivatives of the thermodynamic potential remain continuous while only higher-order derivatives such as the compressibility, the specific heat or the susceptibility are divergent or change discontinuously at the transition point are termed "second-order phase transitions". It is usually for such transitions that the term "critical point" is used. A dominant characteristic of the second-order phase transition is the large increase of the microscopic fluctuations in the vicinity of a critical point which heralds the approaching transition. Fluctuations of density, energy, magnetization, etc., can reach effectively macroscopic magnitudes and correspondingly the related second thermodynamic derivatives and the intensities for the scattering of waves off the system become very large or tend to infinity at certain wavelengths.

The point of interest in the study of critical phenomena both experimentally and theoretically, is the determination of the asymptotic laws governing the approach to a critical point. Nowadays it is customary in the study of critical

phenomena to assume that various quantities of interest have a simple power-law behavior at or near the critical point. For example, in a simple ferromagnet in which the second-order phase transition takes place at H = 0, one assumes that the spontaneous magnetization M behaves asymptotically as

$$M \sim \left(\frac{T_c - T}{T_c}\right)^{\beta} , \qquad (I\text{-}2)$$

where T approaches the critical temperature T_c from below, with β a positive number. The critical point exponent β has a value in the range 0.3-0.5. To be more precise one assumes that the limit

$$\beta = \lim_{\varepsilon \to 0} \{(\log M_s)/\log(\varepsilon)\} \qquad (I\text{-}3)$$

exists. Here ε is defined as

$$\varepsilon \equiv \frac{T_c - T}{T_c} .$$

In our discusion below we shall always employ the shorter and more expressive notation (I-2), with the understanding that (I-3) provides a more precise and realistic definition.

There are many other exponents, which are summarized in Table (I-1). In Table (I-1) C is the specific heat (subscripts H and v for constant magnetic field and constant volume), H the magnetic field, M the magnetization, $\chi = (\partial M/\partial H)_T$ the susceptibility, S the entropy, P the pressure, ρ the density,

Table (I-1) Definitions of critical point exponents.

Quantity	Variable	Exponent	Region
	Fluids		
C_v	ε	$-\alpha'$	$\rho=\rho_c$, $T < T_c$
$\rho_L-\rho_c$	ε	β	coex., $T<T_c$
$\rho_c-\rho_G$	ε	β	coex., $T<T_c$
K_T	ε	$-\gamma'$	coex., $T<T_c$
$\lvert P-P_c\rvert$	$\lvert\rho-\rho_c\rvert$	δ	$T=T_c$
d^2P/dT^2	ε	$-\theta$	coex., $T<T_c$
	Magnetic Systems		
C_H	$-\varepsilon$	$-\alpha$	$H=0$, $T>T_c$
C_H	ε	$-\alpha'$	$H=0$, $T<T_c$
M_S	ε	β	$H=0$, $T<T_c$
χ	$-\varepsilon$	$-\gamma$	$H=0$, $T>T_c$
χ	ε	$-\gamma'$	$H=0$, $T<T_c$
H	M	δ	$H>0$, $T=T_c$
H	M	δ_s	$H>0$, $s=s_c$
s_c-s	M	$1+\xi$	$H>0$, $T=T_c$
$T-T_c$	M	σ	$H>0$, $s=s_c$
$(\partial^{2n+1}M/\partial H^{2n+1})_T$	$-\varepsilon$	$-\gamma_n$	$H=0$, $T>T_c$
ξ	$-\varepsilon$	$-\nu$	$H=0$, $T>T_c$
Γ	r	$2-\eta$	$H=0$, $T=T_c$

K_T the isothermal compressibility, ξ the correlation length and Γ the pair correlation function. A subscript c denotes the value of a quantity at the critical point.

In recent years much study has been done on the subject of critical phase transitions. The results of phenomenological theories and model calculations have shown that some relations exist between different critical exponents. Also it is believed that the knowledge of two or maybe three exponents in a particular system is enough to calculate all the exponents.

Here we shall finish our remarks about the critical phenomena and refer the interested reader to some excellent reviews such as the books, "Phase transitions and critical phenomena" by H. E. Stanley (1971) and "Phase transitions and critical phenomena" edited by C. Domb and M.S. Green (1972-1976). In Chapter V we shall report some experimental results on critical magnetic neutron scattering from $CsMnF_3$ and shall find the magnetic order parameter exponent, β, for $CsMnF_3$.

I-4 Crystal and Magnetic Structure of $CsMnF_3$:

The compounds $XMnF_3$ exist in the pervoskite-type structure when X is Na, K, Rb or NH_4. Simonov et al (1957) showed that, unlike the other triple floride compounds, $CsMnF_3$ has the same structure as hexagonal $BaTiO_3$. X-ray measurements by Zalkin et al in 1962 confirmed this proposed hexagonal structure.

The lattice parameters of the hexagonal cell are $a = 6.213 \pm .003$ Å and $c = 15.074 \pm .004$ Å so that $c/a = 2.426$.

With six formulas per unit cell, the calculated density is 4.84 g/cm^3. The atomic coordinates were given by Zalkin, Lee and Templeton (1962). A sketch of half of the unit cell is shown in Fig. (I-1) and the atomic coordinates are given in Table (I-2). The space group is $P6_3/mmc$. The structure is built up of six closed-packed layers of Cs and F ions with the Mn ions located in the fluorine octahedral holes between the layers. The Cs_2 atoms have 12 fluorine neighbors arranged as in hexagonal close packing; the point symmetry at these sites is $\bar{6}m2(D_{3h})$. The Cs_1 and Cs_3 atoms also have 12 fluorine neighbors, but are arranged as in cubic close packing; the point symmetry at these sites is $3m(C_{3v})$. The interesting feature of this structure is that there are two manganese sites. One-third of the manganese atoms, designated Mn_1 and Mn_4 occupy the centers of fluorine octahedra that share their corners with other octahedra, as in the perovskite structure. The remaining two-thirds of the manganese atoms designated Mn_2 and Mn_3 are in distorted fluorine octahedra that share one face and three corners with other octahedra. Whereas the point symmetry of the Mn_1 and Mn_4 sites is $\bar{3}m(D_{3d})$, the point symmetry about the Mn_2 and Mn_3 sites is $3m(C_{3v})$. The Mn_2 and Mn_3 atoms are distorted out of their close-packed positions to a distance 3.004 Å apart. The distortion of the structure does not affect greatly the various Mn-F distances, but the various F-F distances range from 2.69 to 3.52 Å. The structure of the other half of the cell is analogous to that of the

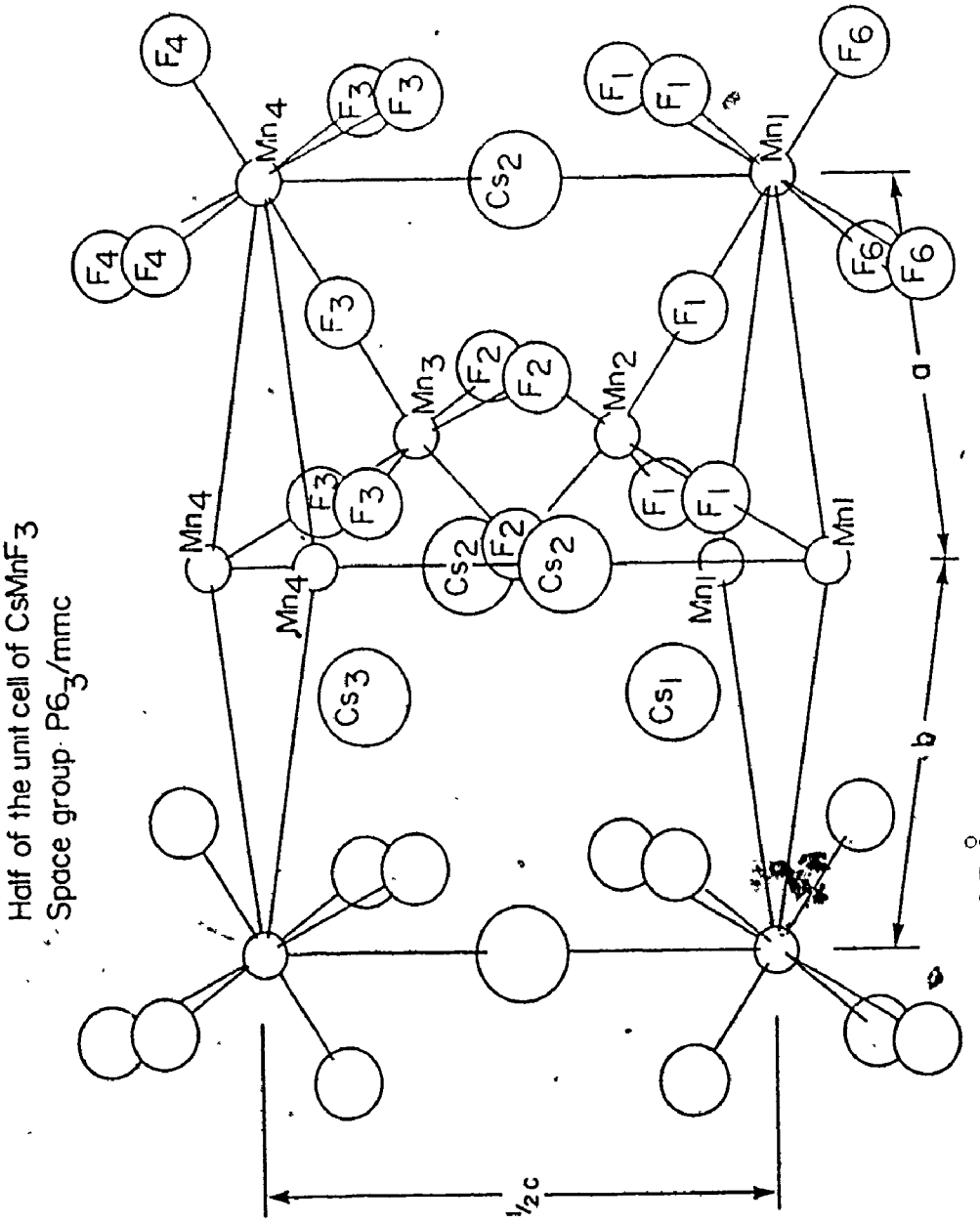

Fig. I-1 Half of the unit cell of $CsMnF_3$.

Table (I-2) Atomic positions and parameters for $CsMnF_3$.

2	Cs_2, Cs_5	in 2b:	$\pm(0,0,\frac{1}{4})$
4	Cs_1, Cs_3, Cs_4, Cs_6	in 4f:	$\pm(\frac{1}{3},\frac{2}{3},z;\frac{2}{3},\frac{1}{3},\frac{1}{2}+z)$ with $z = 0.0986\pm0.0002$
2	Mn_1, Mn_4	in 2a:	$0,0,0;0,0,\frac{1}{2}$
4	Mn_2, Mn_3, Mn_5, Mn_6	in 4f:	$\pm(\frac{1}{3},\frac{2}{3},z;\frac{2}{3},\frac{1}{3},\frac{1}{2}+z)$ with $z = 0.8498\pm0.0004$
6	F_2, F_5	in 6h:	$\pm(x,2x,\frac{1}{4};2x,x,\frac{3}{4},x,\bar{x},\frac{1}{4})$ with $x = 0.522\pm0.002$
12	F_1, F_3, F_4, F_6	in 12k:	$\pm(x,2x,z;2x,x,\bar{z};x,\bar{x},z;x,2x,\frac{1}{2}-z;2x,x,\frac{1}{2}+z;$ $\bar{x},x,\frac{1}{2}+z)$ with $x = 0.835\pm0.002$ and $z = 0.078\pm0.001$

first half; it can be obtained by rotating the first half through 180 degrees about the c axis and translating it $\frac{1}{2}$ c along the c axis.

Below the Néel temperature the magnetic moments associated with the Mn^{2+} ions lie in the plane perpendicular to the hexagonal c axis. The magnetic lattice can be divided into six sublattices in which spins on each sublattice are antiparallel to spins on any adjacent sublattice. The complete magnetic cell of $CsMnF_3$ is shown in Fig. (I-2). This spin arrangement has been confirmed by torsion experiment, antiferromagnetic resonance (AFR) experiments (K. Lee et al 1963), neutron diffraction studies (S.J. Pickart 1963) and by the present work.

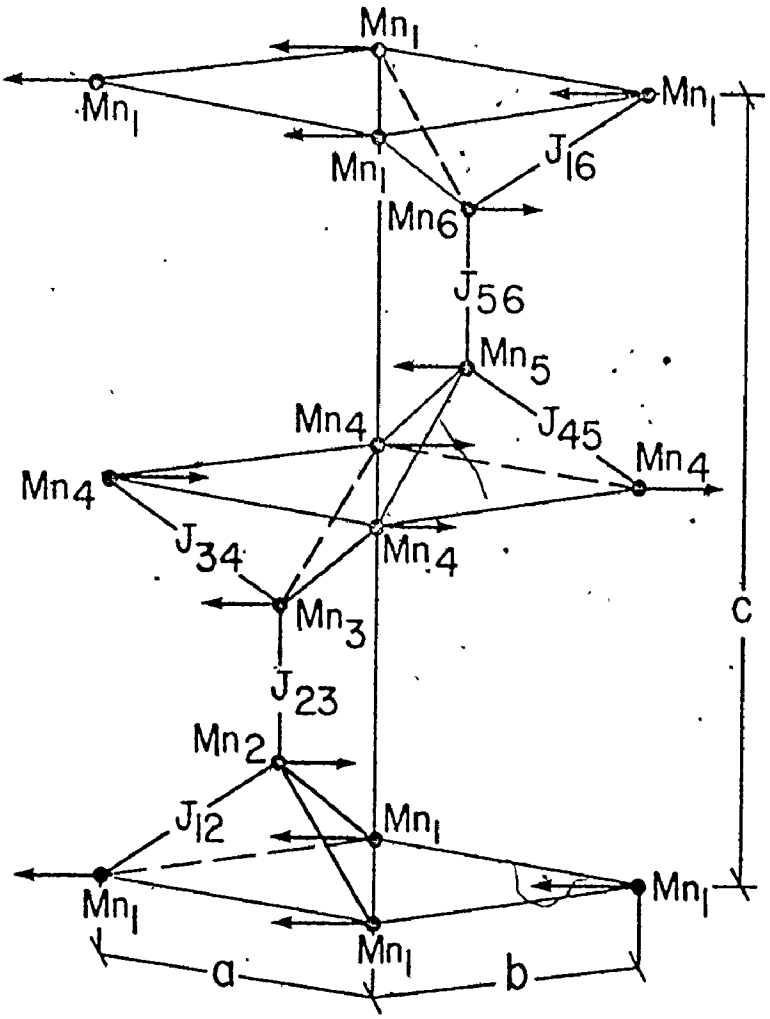

Fig. I-2 Complete magnetic cell of $CsMnF_3$.

CHAPTER II

SPIN WAVE THEORY

It was shown by Bloch (1930) that the low-lying states of spin systems coupled by exchange interactions are wave like. The waves are called spin waves; the energy is quantized and the quantum of energy is called a magnon.

In this chapter we shall study first simple ferromagnetic and antiferromagnetic spin waves and then, the theory will be applied to $CsMnF_3$, which is a more complicated case.

II-1 Spin Waves in a Simple Ferromagnetic System:

A simple ferromagnetic system can be described by the isotropic Heisenberg exchange Hamiltonian

$$H_{ex} = - \sum_{\underline{j},\underline{\delta}} J_{\underline{\delta}} \underline{S}_{\underline{j}} \cdot \underline{S}_{\underline{j}+\underline{\delta}} \qquad \text{(II-1)}$$

where $J_{\underline{\delta}}$ is the exchange integral which is assumed to be positive, $\underline{S}_{\underline{j}}$ is the spin angular momentum operator of the atom at $\underline{j}$ and $\underline{\delta}$ is the vector connecting the atom at $\underline{j}$ to the atom at $\underline{j}+\underline{\delta}$.

Eq. (II-1) can be written in expanded form

$$H_{ex} = - \sum_{\underline{j},\underline{\delta}} J_{\underline{\delta}} [S^x_{\underline{j}} S^x_{\underline{j}+\underline{\delta}} + S^y_{\underline{j}} S^y_{\underline{j}+\underline{\delta}} + S^z_{\underline{j}} S^z_{\underline{j}+\underline{\delta}}] \; . \qquad \text{(II-2)}$$

We shall define z as the equilibrium direction of the ferromagnetic array of spins.

Let us define the spin ladder operators S^+ and S^- as

$$S_j^+ = S_j^x + i\, S_j^y$$
$$S_j^- = S_j^x - i\, S_j^y \quad . \tag{II-3}$$

Using eq. (II-3), eq. (II-2) can be reduced to

$$H_{ex} = - \sum_{j,\delta} J_\delta \left[\frac{1}{2}(S_j^+ S_{j+\delta}^- + S_j^- S_{j+\delta}^+) + S_j^z S_{j+\delta}^z\right]. \tag{II-4}$$

We express the spin operators in terms of the spin deviation operator

$$S_j^+ \equiv (2S)^{\frac{1}{2}}[1-n_j(2S)^{-1}]^{\frac{1}{2}} a_j$$
$$S_j^- \equiv (2S)^{\frac{1}{2}} a_j^+ [1-n_j(2S)^{-1}]^{\frac{1}{2}} \tag{II-5}$$
$$S_j^z \equiv S-n_j$$

where $n_j = a_j^+ a_j$ is the operator of the number of spin deviations, a^+ and a are the boson creation and annihilation operators and they obey the commutation relation

$$[a_i, a_j^+] = \delta_{ij} \quad .$$

This transformation was first used by Holstein and Primakoff and so is called the Holstein-Primakoff transformation (1940).

As $T \to 0$ (i.e. at low temperatures) we know that $\langle a_j^+ a_j \rangle \to 0$ so we can let $(1 - a_j^+ a_j/2S)^{1/2} \approx 1$. Then with this approximation eq's (II-5) will be simplified to

$$S_j^+ = (2S)^{\frac{1}{2}} a_j$$
$$S_j^- = (2S)^{\frac{1}{2}} a_j^+ \qquad \text{(II-6)}$$
$$S_j^z = S - a_j^+ a_j \, .$$

Dyson (1956) and Maleev (1958) developed an alternative form of transformation which we shall not consider here.

Let us substitute eq. (II-6) into eq. (II-4)

$$H_{ex} = - \sum_{j,\underline{\delta}} J_{\underline{\delta}} S^2 - \sum_{j,\underline{\delta}} J_{\underline{\delta}} S [a_j a_{j+\underline{\delta}}^+ + a_j^+ a_{j+\underline{\delta}}$$
$$- a_j^+ a_j - a_{j+\underline{\delta}}^+ a_{j+\underline{\delta}}] \, . \qquad \text{(II-7)}$$

Notice that the quadratic term $a_j^+ a_j a_{j+\underline{\delta}}^+ a_{j+\underline{\delta}}$ has been omitted. This is a good approximation at low temperatures and is in accordance with our previous assumption on reducing eq. (II-5) to eq. (II-6). The first term in the Hamiltonian is constant and is the zero-temperature energy. Since we are going to be concerned with excitations, this term does not concern us.

It is convenient to make a transformation from atomic operators a_j^+, a_j to spin wave operators b_k, b_k^+ defined by

$$b_{\underline{k}}^{+} = N^{-\frac{1}{2}} \sum_{\underline{j}} e^{-i\underline{k}\cdot\underline{j}} a_{\underline{j}}^{+}$$

$$b_{\underline{k}} = N^{-\frac{1}{2}} \sum_{\underline{j}} e^{i\underline{k}\cdot\underline{j}} a_{\underline{j}} \quad . \tag{II-8}$$

where $\underline{j}$ is the position vector of atom j in a Bravais lattice. $b_{\underline{k}}^{+}$ creates a magnon of wave vector $\underline{k}$ and $b_{\underline{k}}$ destroys one. The commutation relations,

$$[b_{\underline{k}}, b_{\underline{k}'}] = [b_{\underline{k}}^{+}, b_{\underline{k}}^{+}] = 0 \quad ; \quad [b_{\underline{k}}, b_{\underline{k}'}^{+}] = \delta_{\underline{k}\underline{k}'} \tag{II-9}$$

can be shown to hold. After the transformation, H_{ex} (eq. (II-7)) assumes the following form:

$$\begin{aligned} H_{ex} &= \text{constant terms} - 2 \sum_{\underline{\delta}} J_{\underline{\delta}} S \sum_{\underline{k}} [b_{\underline{k}}^{+} b_{\underline{k}} (e^{i\underline{k}\cdot\underline{\delta}} - 1)] \\ &= E_o - 2S \sum_{\underline{\delta}} J_{\underline{\delta}} \sum_{\underline{k}} b_{\underline{k}}^{+} b_{\underline{k}} (e^{i\underline{k}\cdot\underline{\delta}} - 1) \qquad \text{(II-10)} \\ &= E_o + 2S \sum_{\underline{k}} b_{\underline{k}}^{+} b_{\underline{k}} [\sum_{\underline{\delta}} J_{\underline{\delta}} (1 - e^{i\underline{k}\cdot\underline{\delta}})] \quad . \end{aligned}$$

So the energy of a magnon with wave vector $\underline{k}$ is

$$E_{\underline{k}} = 2S \sum_{\underline{\delta}} J_{\underline{\delta}} (1 - e^{i\underline{k}\cdot\underline{\delta}}) \quad . \tag{II-11}$$

For a centro symmetric crystal this reduces to

$$E_{\underline{k}} = 2S \sum_{\underline{\delta}} J_{\underline{\delta}} (1 - \cos \underline{k}\cdot\underline{\delta}) \quad .$$

II-2 Spin Waves in a Simple Antiferromagnetic System:

Let us consider a magnetic Bravais lattice which can be divided into two sublattices ℓ and m. Let us also assume that in the equilibrium state all atoms at ℓ sites have spins parallel to the z direction and all the atoms at m sites have spins antiparallel to z direction, with equal number of ℓ and m sites. The Heisenberg exchange Hamiltonian for this lattice can be written as

$$H_{ex} = -\sum_{\ell\ell'}^{\frac{N}{2}} J_{\ell\ell'}\underline{S}_\ell\cdot\underline{S}_{\ell'} - \sum_{mm'}^{\frac{N}{2}} J_{mm'}\underline{S}_m\cdot\underline{S}_{m'} - 2\sum_{\ell,m}^{\frac{N}{2}} J_{\ell m}\underline{S}_\ell\cdot\underline{S}_m \qquad \text{(II-12)}$$

(N.B. in this expression each term is counted twice) where the first term gives the interaction within the ℓ sublattice, the second term gives interaction within the m sublattice and the third term gives the interactions between the two sublattices. Using eq. (II-3) we transform S^x and S^y to, S^+ and S^-, the spin ladder operators. Then

$$H_{ex} = -\sum_{\ell\ell'}^{\frac{N}{2}} J_{\ell\ell'}[\tfrac{1}{2}(S_\ell^+S_{\ell'}^- + S_\ell^-S_{\ell'}^+) + S_\ell^zS_{\ell'}^z] - \sum_{mm'}^{\frac{N}{2}} J_{mm'}[\tfrac{1}{2}(S_m^+S_{m'}^- + S_m^-S_{m'}^+) + S_m^zS_{m'}^z] - 2\sum_{\ell m}^{\frac{N}{2}} J_{m\ell}[\tfrac{1}{2}(S_\ell^+S_m^- + S_\ell^-S_m^+) + S_\ell^zS_m^z] . \qquad \text{(II-13)}$$

Let us now transform S_ℓ^z, S_ℓ^+ and S_ℓ^- to boson operators a_ℓ^+ and a_ℓ,

and S_m^z, S_m^+ and S_m^- to boson operators b_m^+ and b_m according to eqs. (II-6). H_{ex} transforms to

$$
\begin{aligned}
H_{ex} = & - \sum_{\ell\ell'}^{\frac{N}{2}} J_{\ell\ell'}[S(a_\ell a_{\ell'}^+ + a_\ell^+ a_{\ell'}) + S^2 - S(a_\ell^+ a_\ell + a_{\ell'}^+ a_{\ell'})] \\
& - \sum_{mm'}^{\frac{N}{2}} J_{mm'}[S^2 + S(b_m b_{m'}^+ + b_m^+ b_{m'} - b_m^+ b_m - b_{m'}^+ b_{m'})] \\
& - 2 \sum_{\ell m}^{\frac{N}{2}} J_{\ell m}[-S^2 + S(b_m^+ b_m + a_\ell^+ a_\ell) + S(a_\ell b_m + a_\ell^+ b_m^+)] \\
& = \frac{N}{2} S^2 [-\sum_{\ell'}^{\frac{N}{2}} J_{\ell\ell'} - \sum_{m'}^{\frac{N}{2}} J_{mm'} + 2 \sum_{m}^{\frac{N}{2}} J_{\ell m}] \\
& + S \sum_{\ell\ell'}^{\frac{N}{2}} J_{\ell\ell'}[a_\ell^+ a_\ell + a_{\ell'}^+ a_{\ell'} - a_\ell a_{\ell'}^+ - a_\ell^+ a_{\ell'}] \\
& + S \sum_{mm'}^{\frac{N}{2}} J_{mm'}[b_m^+ b_m + b_{m'}^+ b_{m'} - b_m b_{m'}^+ - b_m^+ b_{m'}] \\
& - 2S \sum_{\ell m}^{\frac{N}{2}} J_{m\ell}[b_m^+ b_m + a_\ell^+ a_\ell + a_\ell b_m + a_\ell^+ b_m^+] \, .
\end{aligned}
\tag{II-14}
$$

We transform and write the Hamiltonian in terms of spin wave operators $a_{\underline{k}}$ and $b_{\underline{k}}$. $a_{\underline{k}}$ and $b_{\underline{k}}$ are defined by

$$
a_\ell = (\frac{2}{N})^{\frac{1}{2}} \sum_{\underline{k}} e^{-\underline{k}\cdot\underline{\ell}} a_{\underline{k}} \quad ; \quad b_m = (\frac{2}{N})^{\frac{1}{2}} \sum_{\underline{k}} e^{i\underline{k}\cdot\underline{m}} b_{\underline{k}} \, . \tag{II-15}
$$

Here $\underline{\ell}$ and $\underline{m}$ are the vectors connecting the atoms at ℓ and m sublattices to the origin respectively, and $\underline{k}$ is the reduced wave vector confined to the first Brillouin zone. Using

eq. (II-15) one can show that

$$H_{ex} = \frac{NS^2}{2}[-2J_S(0) + 2J_D(0)]$$

$$+ S \sum_{\underline{k}} [a^+_{\underline{k}}a_{\underline{k}} + b^+_{\underline{k}}b_{\underline{k}}][2J_S(0)-2J_S(\underline{k})-2J_D(0)] \quad \text{(II-16)}$$

$$- 2S \sum_{\underline{k}} J_D(\underline{k})[a_{\underline{k}}b_{\underline{k}} + a^+_{\underline{k}}b^+_{\underline{k}}]$$

where

$$J_S(0) = \sum_{\ell'}^{\frac{N}{2}} J_{\ell\ell'} = \sum_{m'}^{\frac{N}{2}} J_{mm'}$$

$$J_D(0) = \sum_{m}^{\frac{N}{2}} J_{\ell m}$$

$$J_S(\underline{k}) = \sum_{\ell'}^{\frac{N}{2}} J_{\ell\ell'} e^{i\underline{k}\cdot(\underline{\ell}-\underline{\ell}')}$$

$$J_D(\underline{k}) = \sum_{\rho} J(\underline{\rho}) e^{-i\underline{k}\cdot\underline{\rho}} \quad \text{(N.B., } \underline{\rho}=\underline{\ell}-\underline{m}\text{)}.$$

In the eq. (II-16) the first term is constant, the second term is diagonal and represents the interactions within the individual sublattices and the third term is non-diagonal and represents the interactions between the two sublattices. We define

$$B(\underline{k}) = -2S\, J_D(\underline{k})$$

$$A(\underline{k}) = -2S[J_D(0)-J_S(0)+J_S(\underline{k})]$$

$$E_0 = NS^2[-J_S(0)+J_D(0)]$$

and simplify the Hamiltonian to

$$H' = H_{ex} - E_0 = \sum_{\underline{k}} A(\underline{k})\,(a^+_{\underline{k}} a_{\underline{k}} + b^+_{\underline{k}} b_{\underline{k}})$$

$$+ \sum_{\underline{k}} B(\underline{k})\,(a_{\underline{k}} b_{\underline{k}} + a^+_{\underline{k}} b^+_{\underline{k}}) \,. \qquad \text{(II-17)}$$

In order to diagonalize H', we use Bogoliubov's technique (1948) and transform it to a new set of bose operators $\alpha_{\underline{k}}$'s and $\beta_{\underline{k}}$'s which are obtained from linear combinations of $a_{\underline{k}}$'s and $b_{\underline{k}}$'s. We define

$$\begin{aligned} \alpha_{\underline{k}} &= U_{\underline{k}} a_{\underline{k}} + V_{\underline{k}} b^+_{\underline{k}} \\ \beta_{\underline{k}} &= U'_{\underline{k}} a^+_{\underline{k}} + V'_{\underline{k}} b_{\underline{k}} \end{aligned} \qquad \text{(II-18)}$$

and require that H' can be written in diagonal form

$$H' = \sum_{\underline{k}} \lambda_{1\underline{k}} \alpha^+_{\underline{k}} \alpha_{\underline{k}} + \sum_{\underline{k}} \lambda_{2\underline{k}} \beta^+_{\underline{k}} \beta_{\underline{k}} \,. \qquad \text{(II-19)}$$

$\lambda_{1\underline{k}}$ and $\lambda_{2\underline{k}}$ are the magnon energies. The boson operators $\alpha_{\underline{k}}$ and $\beta_{\underline{k}}$ must satisfy the commutation relations

$$\begin{aligned} [\alpha_{\underline{k}}, \alpha^+_{\underline{k}'}] &= [\beta_{\underline{k}}, \beta^+_{\underline{k}'}] = \delta_{\underline{k}\underline{k}'} \\ [\alpha_{\underline{k}}, \beta_{\underline{k}}] &= [\alpha_{\underline{k}}, \beta^+_{\underline{k}}] = 0 \,. \end{aligned} \qquad \text{(II-20)}$$

$\alpha_{\underline{k}}$ and $\beta_{\underline{k}}$ are the annihilation operators for the new states and the new states are the linear combination of the states of different sublattices. Using (II-17)

$$[\alpha_{\underline{k}}, H'] = U_{\underline{k}} A(\underline{k}) a_{\underline{k}} - V_{\underline{k}} A(\underline{k}) b^+_{\underline{k}} + U_{\underline{k}} B(\underline{k}) b^+_{\underline{k}} - V_{\underline{k}} B(\underline{k}) a_{\underline{k}} \,. \qquad \text{(II-21)}$$

Also from (II-19)

$$[\alpha_{\underline{k}}, H'] = \lambda_{1\underline{k}} \alpha_{\underline{k}} = \lambda_{1\underline{k}} (U_{\underline{k}} a_{\underline{k}} + V_{\underline{k}} b_{\underline{k}}^{+}) . \qquad \text{(II-22)}$$

Equating (II-21) and (II-22) we get

$$\begin{aligned} U_{\underline{k}} A(\underline{k}) - V_{\underline{k}} B(\underline{k}) &= \lambda_{1\underline{k}} U_{\underline{k}} \\ U_{\underline{k}} B(\underline{k}) - V_{\underline{k}} A(\underline{k}) &= \lambda_{1\underline{k}} V_{\underline{k}} . \end{aligned} \qquad \text{(II-23)}$$

In order to have non-trivial solutions for $V_{\underline{k}}$ and $U_{\underline{k}}$, the determinant of the above set of equations must vanish.

$$\begin{bmatrix} A(\underline{k}) - \lambda_{1\underline{k}} & -B(\underline{k}) \\ B(\underline{k}) & -A(\underline{k}) - \lambda_{1\underline{k}} \end{bmatrix} = 0 .$$

Then we get

$$\lambda_{1\underline{k}} = \pm \left(A(\underline{k})^2 - B(\underline{k})^2 \right)^{\frac{1}{2}} \qquad \text{(II-24)}$$

as the two degenerate eigenvalues of the isotropic exchange Hamiltonian. Eq. (II-24) shows that the condition for the stability of the model is

$$A(\underline{k}) \geq B(\underline{k}) .$$

V and U can be obtained by substituting $\lambda_{1\underline{k}}$ back into the Eq. (II-23). We get

$$V_{\underline{k}} = \sinh \theta_{\underline{k}} \; ; \; U_{\underline{k}} = \cosh \theta_{\underline{k}}$$

$$B(k) \qquad\qquad A(\underline{k})$$

II-3 Spin Waves In $CsMnF_3$:

In the first part of this section we shall consider a model, described only by an exchange Hamiltonian and in the second part we shall add the effects of dipole-dipole interactions to the original Hamiltonian.

a - The isotropic exchange Hamiltonian:

$CsMnF_3$ is chemically a typical insulating transition metal compound. Only the manganese atoms are magnetic and measurements on similar materials (for a bibliography relating to experimental data on antiferromagnetic substances, see Nagamiya et al 1955) indicate that the coupling between the magnetic moments is mainly superexchange (see Section I-1-b).

We define the lattice translation vector as

$$\underline{R}_n = n_1\underline{a} + n_2\underline{b} + n_3\underline{c} \qquad \text{(II-25)}$$

and the vector connecting the ith atom to the origin of a cell by

$$\underline{\ell}_i = u_i\underline{a} + v_i\underline{b} + w_i\underline{c} \qquad \text{(II-26)}$$

where $\underline{a}$, $\underline{b}$ and $\underline{c}$ are the primitive crystal axes; n_1, n_2 and n_3 are arbitrary integers and u_i, v_i and w_i are the atomic coordinates of ith atom in the cell. The magnetic lattice can be divided into six sublattices, in which the array of spins on each sublattice is antiparallel to the spins on any adjacent sublattice. Details on magnetic structure of

$CsMnF_3$ aregiven in section (I-4).

We assume that the only non zero exchange constants are for the nearest neighbor (n.n.) and second nearest neighbor (s.n.n.) Mn atoms. Let us define J_{nm} as the exchange constant representing the coupling between the nth Mn atom and nearest Mn atom on the mth sublattice. We number the Mn atoms in ascending order in the direction of crystal $\underline{c}$ axis (see fig. (I-2)). By looking at the crystal symmetry of $CsMnF_3$ we can show that there exist only two independent nearest neighbour exchange constants, J_{12} and J_{23}, and only one independent s.n.n. exchange constant J_{35}. The reason is that $J_{45} = J_{16} = J_{34} = J_{12}$, $J_{56} = J_{23}$ and $J_{26} = J_{35}$. Also figure (I-1) shows that, as the n.n.'s there are three Mn_2 atoms coupled to Mn_1 through the F_1 atoms and one Mn_3 atom to Mn_2 through the three F_2 atoms. Similarly the number of n.n. couplings between the remaining Mn atoms can be determined. As the s.n.n.'s Mn_2 atom is coupled to Mn_6 through F_1, Mn_1 and F_6 atoms and Mn_3 atom to Mn_5 through F_3, Mn_4 and F_5 atoms.

Considering the magnetic structure of $CsMnF_3$ and recalling eq. (II-6), we can write the spin operators (S^z, S^+ and S^-) in terms of boson operators (a^+, a) as

$$S_i^z(\underline{R}_n+\underline{\ell}_i) = (-1)^{i-1}[S - a_i^+(\underline{R}_n+\underline{\ell}_i)a(\underline{R}_n+\underline{\ell}_i)]$$

$$S_i^+(\underline{R}_n+\underline{\ell}_i) = (2S)^{\frac{1}{2}}[a_i^+(\underline{R}_n+\underline{\ell}_i)\delta_{i,odd} + a_i(\underline{R}_n+\underline{\ell}_i)\delta_{i,even}] \qquad \text{(II-27)}$$

$$S_i^-(\underline{R}_n+\underline{\ell}_i) = (2S)^{\frac{1}{2}}[a_i^+(\underline{R}_n+\underline{\ell}_i)\delta_{i,even} + a_i(\underline{R}_n+\underline{\ell}_i)\delta_{i,odd}]$$

where

$$\delta_{i,\text{even}} = \begin{cases} 1 & \text{for } i = \text{even number} \\ 0 & \text{for } i = \text{odd number} \end{cases} \quad \text{and}$$

$$\delta_{j,\text{odd}} = \begin{cases} 1 & \text{for } j = \text{odd number} \\ 0 & \text{for } j = \text{even number} \end{cases}$$

Let us assume that there are 6N manganese atoms in the crystal (i.e. N primitive cells).

Recalling eqs. (II-27) and the procedure we followed to get from eq. (II-1) to eq. (II-14) we get the following expanded exchange Hamiltonian in terms of boson operators for $CsMnF_3$

$$\begin{aligned} H_{ex} = E_0 - 2SJ_{12} \{ \sum_{\underline{R}} & a_2^+(\underline{R}+\underline{\ell}_2) a_2(\underline{R}+\underline{\ell}_2) + a_2^+(\underline{R}-\underline{a}-\underline{b}+\underline{\ell}_2) \\ & \times a_2(\underline{R}-\underline{a}-\underline{b}+\underline{\ell}_2) + a_2^+(\underline{R}-\underline{b}-\underline{\ell}_2) a_2(\underline{R}-\underline{b}-\underline{\ell}_2) \\ & + a_6^+(\underline{R}-\underline{a}+\underline{\ell}_6) a_6(\underline{R}-\underline{a}+\underline{\ell}_6) + a_6^+(\underline{R}+\underline{\ell}_6) a_6(\underline{R}+\underline{\ell}_6) \\ & + a_6^+(\underline{R}-\underline{a}-\underline{b}+\underline{\ell}_6) a_6(\underline{R}-\underline{a}-\underline{b}+\underline{\ell}_6) + 6a_1^+(\underline{R}) a_1(\underline{R}) \\ & + [a_1(\underline{R}) a_2(\underline{R}+\underline{\ell}_2) + a_1(\underline{R}) a_2(\underline{R}-\underline{a}-\underline{b}+\underline{\ell}_2) + a_1(\underline{R}) a_2(\underline{R}-\underline{b}+\underline{\ell}_2) \\ & + a_1(\underline{R}) a_6(\underline{R}-\underline{a}+\underline{\ell}_6) + a_1(\underline{R}) a_6(\underline{R}+\underline{\ell}_6) + a_1(\underline{R}) a_6(\underline{R}-\underline{a}-\underline{b}+\underline{\ell}_6) \\ & + \text{C.C.}] \} \end{aligned}$$

(equation continued next page)

$$
\begin{aligned}
&-2S\{\sum_{\underline{R}} J_{23} a_2^+(\underline{R}+\underline{\ell}_2)\, a_2(\underline{R}+\underline{\ell}_2) \\
&+ J_{12}[a_4^+(\underline{R}+\underline{\ell}_4)\, a_4(\underline{R}+\underline{\ell}_4) + a_4^+(\underline{R}+\underline{b}+\underline{\ell}_4)\, a_4(\underline{R}+\underline{b}+\underline{\ell}_4) \\
&+ a_4^+(\underline{R}+\underline{b}+\underline{a}+\underline{\ell}_4)\, a_4(\underline{R}+\underline{\ell}_4+\underline{a}+\underline{b})] + (J_{23}+3J_{12})\, a_3^+(\underline{R}+\underline{\ell}_3)\, a_3(\underline{R}+\underline{\ell}_3) \\
&+ [J_{23} a_3(\underline{R}+\underline{\ell}_3)\, a_2(\underline{R}+\underline{\ell}_2) + J_{12}\{a_3(\underline{R}+\underline{\ell}_3)\, a_4(\underline{R}+\underline{\ell}_4) \\
&+ a_3(\underline{R}+\underline{\ell}_3)\, a_4(\underline{R}+\underline{b}+\underline{\ell}_4) + a_3(\underline{R}+\underline{\ell}_3)\, a_4(\underline{R}+\underline{b}+\underline{a}+\underline{\ell}_4)\} \\
&+ \text{C.C.}]\} \\
&-2S\{\sum_{\underline{R}} J_{23} a_6^+(\underline{R}+\underline{\ell}_6)\, a_6(\underline{R}+\underline{\ell}_6) + J_{12}[a_4^+(\underline{R}+\underline{\ell}_4)\, a_4(\underline{R}+\underline{\ell}_4) \\
&+ a_4^+(\underline{R}+\underline{a}+\underline{b}+\underline{\ell}_4)\, a_4(\underline{R}+\underline{\ell}_4+\underline{a}+\underline{b}) + a_4^+(\underline{R}+\underline{a}+\underline{\ell}_4)\, a_4(\underline{R}+\underline{a}+\underline{\ell}_4)] \qquad \text{(II-28)} \\
&+ (J_{23}+3J_{12})\, a_5^+(\underline{R}+\underline{\ell}_5)\, a_5(\underline{R}+\underline{\ell}_5) \\
&+ [J_{23} a_5(\underline{R}+\underline{\ell}_5)\, a_6(\underline{R}+\underline{\ell}_6) + J_{12}\{a_5(\underline{R}+\underline{\ell}_5)\, a_4(\underline{R}+\underline{\ell}_4) \\
&+ a_5(\underline{R}+\underline{\ell}_5)\, a_4(\underline{R}+\underline{\ell}_4+\underline{a}+\underline{b}) + a_5(\underline{R}+\underline{\ell}_5)\, a_4(\underline{R}+\underline{\ell}_4+\underline{a})\} \\
&+ \text{C.C.}]\} \\
&-2SJ_{35}\{\sum_{\underline{R}} 3a_3^+(\underline{R}+\underline{\ell}_3)\, a_3(\underline{R}+\underline{\ell}_3) + a_5^+(\underline{R}+\underline{\ell}_5)\, a_5(\underline{R}+\underline{\ell}_5) \\
&+ a_5^+(\underline{R}+\underline{\ell}_5-\underline{a})\, a_5(\underline{R}+\underline{\ell}_5-\underline{a}) + a_5^+(\underline{R}+\underline{\ell}_5-\underline{b})\, a_5(\underline{R}+\underline{\ell}_5-\underline{b}) \\
&+ 3a_2^+(\underline{R}+\underline{\ell}_2)\, a_2(\underline{R}+\underline{\ell}_2) + a_6^+(\underline{R}+\underline{\ell}_6-\underline{c})\, a_6(\underline{R}+\underline{\ell}_6-\underline{c}) \\
&+ a_6^+(\underline{R}+\underline{\ell}_6-\underline{c}-\underline{a})\, a_6(\underline{R}+\underline{\ell}_6-\underline{c}-\underline{a}) + a_6^+(\underline{R}+\underline{\ell}_6-\underline{c}-\underline{b})\, a_6(\underline{R}+\underline{\ell}_6-\underline{c}-\underline{b}) \\
&- [a_3(\underline{R}+\underline{\ell}_3)\{a_5^+(\underline{R}+\underline{\ell}_5) + a_5^+(\underline{R}+\underline{\ell}_5-\underline{a}) + a_5^+(\underline{R}+\underline{\ell}_5-\underline{b})\} \\
&+ a_2^+(\underline{R}+\underline{\ell}_2)\{a_6(\underline{R}+\underline{\ell}_6-\underline{c}) + a_6(\underline{R}+\underline{\ell}_6-\underline{c}-\underline{a}) + a_6(\underline{R}+\underline{\ell}_6-\underline{c}-\underline{b})\} \\
&+ \text{C.C.}]\}
\end{aligned}
$$

where C.C. in each bracket means all the Hermitian conjugates of the terms in that bracket . Also notice that we have used $\underline{R}$ instead of $\underline{R}_n$. In order to transform from bose operators, $a_{\underline{R}}$ and $a^+_{\underline{R}}$, to spin wave operators, $b_{\underline{k}}$ and $b^+_{\underline{k}}$, we define the following transformation equation

$$a_j(\underline{R}+\underline{\ell}_j) = \frac{1}{(N)^{\frac{1}{2}}} \sum_{\underline{k}} e^{(-1)^j i\underline{k}\cdot(\underline{R}+\underline{\ell}_j)} b_j(\underline{k}) \quad . \qquad \text{(II-29)}$$

where $b_j(\underline{k})$ satisfies the commutation relations (II-9). We substitute eq. (II-29) into the Hamiltonian (II-28) and follow the steps taken in section (II-2) for the simple antiferromagnetic case, and let $b_j(\underline{k}) = b_j$. Then we get

$$\begin{aligned} H_{ex} = E_0 + \sum_{\underline{k}} \{ & A_1(2b_1^+b_1+b_2^+b_2+b_3^+b_3+2b_4^+b_4+b_5^+b_5+b_6^+b_6) \\ & + A_4(b_2^+b_2+b_3^+b_3+b_5^+b_5+b_6^+b_6) \\ & + A_{10}(b_3^+b_3+b_2^+b_2+b_5^+b_5+b_6^+b_6) \\ & + [A_2(\underline{k})b_1b_2+A_3^*(\underline{k})b_1^+b_6^+ \\ & + [A_6(\underline{k})(b_3b_2+b_5^+b_6^+)+A_7(\underline{k})b_3b_4 \\ & + A_9(\underline{k})b_5b_4+A_{11}(\underline{k})b_3b_5^+ \\ & + A_{12}(\underline{k})b_2^+b_6 + \text{C.C.}]\}^* \end{aligned} \qquad \text{(II-30)}$$

where

$$A_1 = -6SJ_{12}$$

$$A_2(\underline{k}) = -2SJ_{12}[e^{i\underline{k}\cdot\underline{\ell}_2}+e^{i\underline{k}\cdot(\underline{\ell}_2-\underline{b})}+e^{i\underline{k}\cdot(\underline{\ell}_2-\underline{a}-\underline{b})}]$$

$$A_3(\underline{k}) = -2SJ_{12}[e^{i\underline{k}\cdot(\underline{\ell}_6-\underline{a}-\underline{c})}+e^{i\underline{k}\cdot(\underline{\ell}_6-\underline{c})}+e^{i\underline{k}\cdot(\underline{\ell}_6-\underline{a}-\underline{b}-\underline{c})}]$$

$$A_4 = -2SJ_{23}$$

$$A_6(\underline{k}) = -2SJ_{23}e^{i\underline{k}\cdot(\underline{\ell}_2-\underline{\ell}_3)}$$

$$A_7(\underline{k}) = -2SJ_{12}[e^{i\underline{k}\cdot(\underline{\ell}_4-\underline{\ell}_3)}+e^{i\underline{k}\cdot(\underline{\ell}_4+\underline{b}+\underline{\ell}_3)}+e^{i\underline{k}\cdot(\underline{\ell}_4+\underline{b}+\underline{a}-\underline{\ell}_3)}]$$

$$A_9(\underline{k}) = -2SJ_{12}[e^{i\underline{k}\cdot(\underline{\ell}_4-\underline{\ell}_5)}+e^{i\underline{k}\cdot(\underline{\ell}_4+\underline{b}+\underline{a}-\underline{\ell}_5)}+e^{i\underline{k}\underline{\ell}(\underline{\ell}_4+\underline{a}-\underline{\ell}_5)}]$$

$$A_{10} = -6SJ_{35}$$

$$A_{11}(\underline{k}) = 2SJ_{35}[e^{i\underline{k}\cdot(\underline{\ell}_5-\underline{\ell}_3)}+e^{i\underline{k}\cdot(\underline{\ell}_5-\underline{a}-\underline{\ell}_3)}+e^{i\underline{k}\cdot(\underline{\ell}_5+\underline{b}-\underline{\ell}_3)}]$$

$$A_{12}(\underline{k}) = 2SJ_{35}[e^{i\underline{k}\cdot(\underline{\ell}_6-\underline{c}-\underline{\ell}_2)}+e^{i\underline{k}\cdot(\underline{\ell}_6-\underline{c}-\underline{a}-\underline{\ell}_2)}+e^{i\underline{k}\cdot(\underline{\ell}_6-\underline{c}+\underline{b}-\underline{\ell}_2)}]$$

We diagonalize the Hamiltonian (II-30) using Bogoliubov's technique in a general form to that given in the previous section. Let us construct new bose operators, α_k's, from linear combinations of spin wave operators, b_k's.

$$\alpha_{\underline{k}} = c_1b_1+c_2b_2^+ +c_3b_3+c_4b_4^+ +c_5b_5+c_6b_6^+ . \qquad \text{(II-31)}$$

$\alpha_{\underline{k}}$ obeys the commutation relation

$$[\alpha_{\underline{k}},\alpha_{\underline{k}'}^+] = \delta_{\underline{k}\underline{k}'} . \qquad \text{(II-32)}$$

Then we require the Hamiltonian (II-30) to be written in the form

$$H_{ex} = E_0 + \sum_{\underline{k}} \lambda_{\underline{k}} \alpha^+_{\underline{k}} \alpha_{\underline{k}} \qquad \text{(II-33)}$$

where $\lambda_{\underline{k}}$ is the spin wave energy of the state with vector $\underline{k}$.

From equations (II-32), (II-33) and (II-31) we get

$$\begin{aligned} [\alpha_{\underline{k}}, H_{ex}] &= \lambda_{\underline{k}} \alpha_{\underline{k}} \\ &= \lambda_{\underline{k}} (c_1 b_1 + c_2 b_2^+ + c_3 b_3 + c_4 b_4^+ + c_5 b_5 + c_6 b_6^+) \ , \end{aligned} \qquad \text{(II-34)}$$

But from (II-30) we get

$$\begin{aligned} [\alpha_{\underline{k}}, H_{ex}] = {} & b_1 [2A_1 c_1 - A_2(\underline{k}) c_2 - A_3(\underline{k}) c_6] \\ & + b_2^+ [A_2^*(\underline{k}) c_1 - A_1 c_2 + A_6^*(\underline{k}) c_3 - A_4 c_2 - A_{10} c_2 - A_{12}(\underline{k}) c_6] \\ & + b_3 [-A_6(\underline{k}) c_2 + (A_1 + A_4) c_3 - A_7(\underline{k}) c_4 + A_{10} c_3 + A_{11}(\underline{k}) c_5] \\ & + b_4^+ [A_7^*(\underline{k}) c_3 - 2A_1 c_4 + A_9^*(\underline{k}) c_5] \\ & + b_5 [-A_9(\underline{k}) c_4 + (A_1 + A_4) c_5 - A_6^*(\underline{k}) c_6 + A_{10} c_5 + A_{11}^*(\underline{k}) c_3] \\ & + b_6^+ [A_3(\underline{k}) c_1 + A_6(\underline{k}) c_5 - (A_1 + A_4 - A_{10}) c_6 - A_{12}^*(\underline{k}) c_2] \ . \end{aligned} \qquad \text{(II-35)}$$

Finally, similarly to the simple antiferromagnetic case we get

$$\begin{pmatrix} (2A_1-\lambda_{\underline{k}}) & -A_2(\underline{k}) & 0 & 0 & 0 & -A_3(\underline{k}) \\ A_2^*(\underline{k}) & -A_1-A_4-A_{10}-\lambda_{\underline{k}}) & A_6^*(\underline{k}) & 0 & 0 & -A_{12}(\underline{k}) \\ 0 & -A_6(\underline{k}) & (A_1+A_4+A_{10}-\lambda_{\underline{k}}) & -A_7(\underline{k}) & A_{11}(\underline{k}) & 0 \\ 0 & 0 & A_7^*(\underline{k}) & (-2A_1-\lambda_{\underline{k}}) & A_9^*(\underline{k}) & 0 \\ 0 & 0 & A_{11}^*(\underline{k}) & -A_9(\underline{k}) & (A_1+A_4+A_{10}-\lambda_{\underline{k}}) & -A_6^*(\underline{k}) \\ A_3^*(\underline{k}) & -A_{12}^*(\underline{k}) & 0 & 0 & A_6(\underline{k}) & (-A_1-A_4-A_{10}-\lambda_{\underline{k}}) \end{pmatrix} = 0 \qquad \text{(II-36)}$$

where all the non-diagonal elements are complex. This matrix equation can be solved numerically for any given wave vector $\underline{k}$ if the exchange constants are specified. There are six real solutions for the eigenvalue $\lambda_{\underline{k}}$, given wave vector $\underline{k}$. Due to the anti-Hermitian symmetry, for each solution $\lambda_{\underline{k}}$ there is also a solution $-\lambda_{\underline{k}}$. There are three branches of the dispersion curves and the states, are degenerate as in the simple antiferromagnet described in the previous section.

b - The effects of dipole-dipole interactions on the spin waves in $CsMnF_3$:

In the last subsection we determined the spin wave energies in $CsMnF_3$ for the isotropic exchange Hamiltonian. Like most actual physical systems, $CsMnF_3$ also has anisotropic interac-

tions. These arise mainly from magnetic dipole-dipole interaction and spin-orbit coupling. Spin-orbit couplings are not normally important in Mn^{2+} ions and magnetic dipole-diple interactions are the most likely source of anisotropy. In this section we shall determine the effects of dipole-dipole interactions on the spin wave dispersion curves.

We take the total Hamiltonian H_T as given by

$$H_T = H_{ex} + H_{d-d}$$

where H_{d-d} represents the dipole-dipole interactions and H_{ex} is the exchange Hamiltonian which was treated in the previous subsection. The magnetic dipole-dipole interactions are given by (R. M. White 1970)

$$H_{d-d} = \frac{g^2\mu_B^2}{2} \sum_{u,u'} \frac{1}{r^5} [r^2(\underline{S}_u \cdot \underline{S}_{u'}) - 3(\underline{S}_u \cdot \underline{r})(\underline{S}_{u'} \cdot \underline{r})] \quad \text{(II-37)}$$

where μ_B is the Bohr magneton, g is the Landé factor, $\underline{S}_u$ is the spin associated with atom at position $\underline{u}$ and $\underline{r}$ is the vector connecting $\underline{u}$ to $\underline{u}'$ (i.e. $\underline{r} = \underline{u} - \underline{u}'$). We define

$$r^+ = x + iy \quad ; \quad r^- = x - iy \,. \quad \text{(II-38)}$$

Equation (II-37) can be simplified by rearranging the terms and noting that

$$r^- r^+ = r^+ r^- = r^2 - z^2 \,.$$

$$H_{d-d} = \frac{g^2\mu_B^2}{2} \sum_{uu'} \{\frac{1}{r^5} [(r^2-3z^2)S_u^zS_{u'}^z + \frac{1}{4}(S_u^+S_{u'}^- + S_u^-S_{u'}^+)$$

$$\times (3z^2-r^2) - \frac{3}{2} r^-(S_u^zS_{u'}^+ + S_u^+S_{u'}^z)$$

$$- \frac{3}{2} zr^+(S_u^zS_{u'}^- + S_u^-S_{u'}^z) - \frac{3}{4} (S_u^+S_{u'}^+[r^-]^2$$

$$+ S_u^-S_{u'}^-[r^+]^2)]\} .$$

Since we have assumed z to be the equilibrium direction of the spin, the stability condition demands that the terms linear in x and y vanish, so that at equilibrium

$$H_{d-d} = \frac{g^2\mu_B^2}{2} \sum_{uu'} \{\frac{1}{r^5} [(r^2-3z^2)S_u^zS_{u'}^z$$

$$+ \frac{1}{4} (S_u^+S_{u'}^- + S_u^-S_{u'}^+)(3z^2-r^2) \qquad \text{(II-39)}$$

$$- \frac{3}{4} (S_u^+S_{u'}^+[r^-]^2 + S_u^-S_{u'}^-[r^+]^2)]\}$$

Experiments by Lee et al (1963) show that a large axial anisotropy along the c axis and a weak sixfold anisotropy in the transverse plane confine the spin to the crystal (1,2,0) direction. This preferred axis is assumed to be the equilibrium direction (z) of the spin.

Let us define

$$E_{\underline{r}} = \frac{g^2\mu_B^2}{2} (\frac{3z^2-r^2}{r^5}) \quad ; \quad B_{\underline{r}} = -\frac{3}{8} g^2\mu_B^2 \frac{(r-)^2}{r^5} .$$

Then we can rewrite

$$H_{d-d} = -2 \sum_{uu'} E_{\underline{r}} S_u^z S_{u'}^z$$

$$+ \frac{1}{2} E_{\underline{r}} (S_u^+ S_{u'}^- + S_u^- S_{u'}^+)$$

$$+ B_{\underline{r}} S_u^+ S_{u'}^+ + B_{\underline{r}}^* S_u^- S_{u'}^- \,.$$

We split the summation over $\underline{u}$ to summation over $\underline{R}_n$ and $\underline{\ell}_i$ and $\underline{u}'$ to $\underline{R}_{n'}$ and $\underline{\ell}_j$ ($\underline{R}_n$ and ℓ_i have been defined by eqs (II-25) and (II-26)). In order to reduce the number of subscripts we shall use $\underline{n}$ instead of $\underline{R}_n$ and $\underline{i}$ instead of $\underline{\ell}_i$.

Let us redefine

$$E_{\underline{r}} = E_{\underline{nn'ij}} = E_{\underline{dij}}$$
$$B_{\underline{r}} = B_{\underline{nn'ij}} = B_{\underline{dij}} \qquad \text{(II-40)}$$

where $\underline{d} = \underline{n}' - \underline{n} = \underline{R}_{n'} - \underline{R}_n$. Now let us define the Fourier transform of $E_{\underline{ijd}}$ and $B_{\underline{ijd}}$

$$E_{\underline{ijk}} = \sum_{\underline{d}} E_{\underline{ijd}} e^{i\underline{k}\cdot(\underline{\ell}_i - \underline{\ell}_j - \underline{d})}$$
$$B_{\underline{ijk}} = \sum_{\underline{d}} B^*_{\underline{ijd}} e^{i\underline{k}\cdot(\underline{\ell}_i - \underline{\ell}_j - \underline{d})} \,. \qquad \text{(II-41)}$$

Using eqs. (II-29), (II-40), (II-41) and going through some manipulations, the Hamiltonian can be transformed to

$$H_{d-d} = -2S^2 \sum_{\underline{n}dij} E_{ijd}$$

$$+2S \sum_{\underline{k}} \{[\sum_{i} b_i^+(\underline{k}) b_i(\underline{k}) \sum_{jd} E_{ijd}(-1)^{i-j}$$

$$+ \sum_{j} b_j^+(\underline{k}) b_j(\underline{k}) \sum_{id} E_{ijd}(-1)^{i-j}]\}$$

$$+ S \sum_{ij\underline{k}} \{b_i^+(\underline{k}) b_j(\underline{k}) E_{ij\underline{k}} \delta_{(i-j),\text{even}}$$

$$+ b_i^+(\underline{k}) b_j^+(\underline{k}) E_{ij\underline{k}} \delta_{i,\text{odd}} \delta_{j,\text{even}}$$

$$+ b_i^+(\underline{k}) b_j^+(\underline{k}) E^*_{ij\underline{k}} \delta_{i,\text{even}} \delta_{j,\text{odd}} + \text{C.C.}\}$$

$$+2S \sum_{ij\underline{k}} \{B^*_{ij\underline{k}} [b_i(\underline{k}) b_j(-\underline{k}) \delta_{i,\text{odd}} \delta_{j,\text{even}}$$

$$+ b_i(\underline{k}) b_j^+(-\underline{k}) \delta_{i,\text{odd}} \delta_{j,\text{even}}$$

$$+ b_i^+(\underline{k}) b_j(-\underline{k}) \delta_{i,\text{even}} \delta_{j,\text{odd}}$$

$$+ b_i^+(\underline{k}) b_j^+(-\underline{k}) \delta_{i,\text{even}} \delta_{j,\text{odd}}] + \text{C.C.}\}$$

where C.C. means Hermitian conjugate of the terms in the brackets, and

$$\delta_{i,\text{even}} = \begin{cases} 1 \text{ for } i = \text{even number} \\ 0 \text{ for } i = \text{odd number} \end{cases} \quad \text{and}$$

$$\delta_{j,\text{odd}} = \begin{cases} 1 \text{ for } j = \text{odd number} \\ 0 \text{ for } j = \text{even number} \end{cases}$$

Then recalling eq. (II-30) the total Hamiltonian can be written as

$$H_T = H_{ex} + H_{d-d} = E_0 + E_0' + \sum_{\underline{k}} H_{ex}(\underline{k}) + H_{d-d}(\underline{k})$$

where E_0 is defined before and $E_0' = -2S^2 \sum_{dij} E_{ijd}$, the constant term in H_{d-d}. Of course for the sake of saving some space we have not written H_T in expanded form.

Symmetrizing the Hamiltonian with $\underline{k}$ restricted to only positive values in the summation we get

$$H_{TS} = E_0+E_0' + \sum_{\underline{k}} H_{ex}(\underline{k})+H_{ex}(-\underline{k})+H_{d-d}(\underline{k})+H_{d-d}(-\underline{k}). \quad \text{(II-42)}$$

Now we define $\alpha_{\underline{k}}$ in terms of suitable linear combination of operators $b_i(\underline{k})$ and $b_i^+(\underline{k})$ with coefficients c_i and c_i'

$$\begin{aligned}\alpha_{\underline{k}} = {} & c_1 b_1(\underline{k})+c_1' b_1^+(-\underline{k})+c_2 b_2^+(\underline{k})+c_2' b_2(-\underline{k}) \\ & + c_3 b_3(\underline{k})+c_3' b_3^+(-\underline{k})+c_4 b_4^+(\underline{k})+c_4' b_4(-\underline{k}) \\ & + c_5 b_5(\underline{k})+c_5' b_5^+(-\underline{k})+c_6 b_6^+(\underline{k})+c_6' b_6(-\underline{k})\end{aligned}$$

which diagonalizes the symmetrized Hamiltonian (II-42) with eigenvalue $\lambda_{\underline{k}}$

$$[\alpha_{\underline{k}}, H_{TS}] = \lambda_{\underline{k}}\alpha_{\underline{k}} = \lambda_{\underline{k}}[c_1 b_1(\underline{k})+c_1' b_1^+(-k)+\ldots.+c_6' b_6(-\underline{k})] .$$

Finally following the procedure we used to get from eq. (II-34) to (II-36), we get the following matrix equation

which gives the eigenvalue $\lambda_{\underline{k}}$

[The matrix is given in the next page] = 0 (II-43)

where $M_1 = 4E_{10}+2E_{11}(\underline{k})+2A_1$ and $M_2 = 4E_{20}+2E_{11}(\underline{k})+A_1+A_4+A_{10}$. A_1 to A_{12}, $E_{ij}(\underline{k})$ and $B_{ij}(\underline{k})$ have been defined earlier. The diagonal terms $E_{10} = \sum_{J=1}^{6} E_{1j}(\underline{k}=0)$.

It can be shown that

$$E_{30} = E_{10} = (E_{11}, 2E_{12}-2E_{13}-E_{14})_{\underline{k}=0}$$

$$E_{60} = E_{50} = E_{30} = E_{20} = (E_{11}-F_{12}+E_{13}-E_{23}-E_{25}+E_{26})_{\underline{k}=0}.$$

We write $E_{ij}(\underline{k})$ and $B_{ij}(\underline{k})$ in terms of dipole sums, $D_{ij}^{\alpha\beta}(\underline{k})$

$$E_{ij}(\underline{k}) = -c[D_{ij}^{zz}(\underline{k})/4 \qquad \text{(II-44)}$$

$$B_{ij}(\underline{k}) = c[D_{ij}^{xx}(\underline{k})-D_{ij}^{yy}(\underline{k})-2iD_{ij}^{xy}(\underline{k})]/8$$

where

$$D_{ij}^{\alpha\beta}(\underline{k}) = \sum_{ij} \frac{1}{r_{ij}^5}[3r_{ij}^{\alpha}r_{ij}^{\beta} - r_{ij}^2]\exp(i\underline{k}\cdot\underline{r}_{ij}) ,$$

$c = S.\ g^2\mu_B^2$/volume of the cell

$= 0.000258$ THz for $CsMnF_3$,

α and β represent any one of the three cartesian coordinates x, y and z.

$M_1-\lambda_{\underline{k}}$	$-4B^*_{11}(\underline{k})$	$-2E^*_{12}(\underline{k})$ $-A_2(\underline{k})$	$4B^*_{12}(\underline{k})$	$2E^*_{13}(\underline{k})$	$-4B^*_{13}(\underline{k})$	$-2E^*_{14}(\underline{k})$	$4B^*_{14}(\underline{k})$	$2E^*_{15}(\underline{k})$	$-4B^*_{15}(\underline{k})$	$-2E^*_{16}(\underline{k})$ $-A^*_2(\underline{k})$	$4B^*_{16}(\underline{k})$
$4B_{11}(\underline{k})$	$-M_1-\lambda_{\underline{k}}$	$-4B_{12}(-\underline{k})$	$2E^*_{12}(\underline{k})$ $+A_2(\underline{k})$	$4B_{13}(-\underline{k})$	$-2E^*_{13}(\underline{k})$	$-4B_{14}(-\underline{k})$	$2E^*_{14}(\underline{k})$	$4B_{15}(-\underline{k})$	$-2E^*_{15}(\underline{k})$	$-4B_{16}(-\underline{k})$	$2E^*_{16}(\underline{k})$ $+A^*_2(\underline{k})$
$2E_{12}(\underline{k})$ $+A^*_2(\underline{k})$	$-4B^*_{12}(-\underline{k})$	$-M_2-\lambda_{\underline{k}}$	$4B^*_{22}(\underline{k})$	$2E^*_{23}(\underline{k})$ $+A^*_6(\underline{k})$	$-4B^*_{23}(\underline{k})$	$-2E^*_{24}(\underline{k})$	$4B^*_{24}(\underline{k})$	$2E^*_{25}(\underline{k})$	$-4B^*_{25}(\underline{k})$	$-2E^*_{26}(\underline{k})$ $-A^*_{12}(\underline{k})$	$4B^*_{26}(\underline{k})$
$4B_{12}(\underline{k})$	$-E_{12}(\underline{k})$ $-A^*_2(\underline{k})$	$-4B_{22}(\underline{k})$	$M_2-\lambda_{\underline{k}}$	$4B_{23}(-\underline{k})$	$-2E^*_{23}(\underline{k})$ $-A^*_6(\underline{k})$	$-4B_{24}(-\underline{k})$	$2E_{24}(\underline{k})$	$4B_{25}(-\underline{k})$	$-2E^*_{25}(\underline{k})$	$-4B_{26}(-\underline{k})$	$2E_{26}(\underline{k})$ $+A_{12}(\underline{k})$
$2E_{13}(\underline{k})$	$-4B^*_{13}(-\underline{k})$	$-2E_{23}(\underline{k})$ $-A_6(\underline{k})$	$4B^*_{23}(-\underline{k})$	$M_2-\lambda_{\underline{k}}$	$-4B^*_{33}(\underline{k})$	$-2E_{34}(\underline{k})$ $-A_7(\underline{k})$	$4B^*_{34}(\underline{k})$	$2E^*_{35}(\underline{k})$ $+A_{11}(\underline{k})$	$-4B^*_{35}(\underline{k})$	$-2E_{36}(\underline{k})$	$4B_{36}(\underline{k})$
$4B_{13}(\underline{k})$	$-2E_{13}(\underline{k})$	$-4B_{23}(\underline{k})$	$2E_{23}(\underline{k})$ $+A_6(\underline{k})$	$4B_{33}(\underline{k})$	$-M_2-\lambda_{\underline{k}}$	$-4B_{34}(-\underline{k})$	$2E^*_{34}(\underline{k})$ $+A_7(\underline{k})$	$4B_{35}(-\underline{k})$	$-2E^*_{35}(\underline{k})$ $-A_{11}(\underline{k})$	$-4B_{36}(-\underline{k})$	$2E^*_{36}(\underline{k})$
$2E_{14}(\underline{k})$	$-4B^*_{14}(-\underline{k})$	$-2E^*_{24}(\underline{k})$	$4B^*_{24}(-\underline{k})$	$2E_{34}(\underline{k})$ $+A^*_7(\underline{k})$	$-4B^*_{34}(-\underline{k})$	$-M_1-\lambda_{\underline{k}}$	$4B^*_{44}(\underline{k})$	$2E^*_{45}(\underline{k})$ $+A_7(\underline{k})$	$-4B^*_{45}(\underline{k})$	$-2E_{46}(\underline{k})$	$4B^*_{46}(\underline{k})$
$4B_{14}(\underline{k})$	$-2E_{14}(\underline{k})$	$-4B_{24}(\underline{k})$	$2E_{24}(\underline{k})$	$4B_{34}(\underline{k})$	$-2E_{34}(\underline{k})$ $-A^*_7(\underline{k})$	$-4B_{44}(\underline{k})$	$M_1-\lambda_{\underline{k}}$	$4B_{45}(-\underline{k})$	$-2E^*_{45}(\underline{k})$ $-A_7(\underline{k})$	$-4B_{46}(-\underline{k})$	$2E_{46}(\underline{k})$
$2E_{15}(\underline{k})$	$-4B^*_{15}(-\underline{k})$	$-2E_{25}(\underline{k})$	$4B^*_{25}(-\underline{k})$	$2E_{35}(\underline{k})$ $+A^*_{11}(\underline{k})$	$-4B^*_{35}(-\underline{k})$	$-2E_{45}(\underline{k})$ $-A^*_7(\underline{k})$	$4B^*_{45}(-\underline{k})$	$M_2-\lambda_{\underline{k}}$	$-4B^*_{55}(\underline{k})$	$-2E^*_{56}(\underline{k})$ $-A^*_6(\underline{k})$	$4B^*_{56}(\underline{k})$
$4B_{15}(\underline{k})$	$-2E_{15}(\underline{k})$	$-4B_{25}(\underline{k})$	$2E_{25}(\underline{k})$	$4B_{35}(\underline{k})$	$-2E_{35}(\underline{k})$ $-A^*_{11}(\underline{k})$	$-4B_{45}(\underline{k})$	$2E_{45}(\underline{k})$ $+A^*_7(\underline{k})$	$4B_{55}(\underline{k})$	$-M_2-\lambda_{\underline{k}}$	$-4B_{56}(-\underline{k})$	$2E_{56}(\underline{k})$ $+A_6(\underline{k})$
$2E_{16}(\underline{k})$ $+A_2(\underline{k})$	$-4B^*_{16}(-\underline{k})$	$-2E^*_{26}(\underline{k})$ $-A^*_{12}(\underline{k})$	$4B^*_{26}(-\underline{k})$	$2E_{36}(\underline{k})$	$-4B^*_{36}(-\underline{k})$	$-2E^*_{46}(\underline{k})$	$4B^*_{46}(-\underline{k})$	$2E_{56}(\underline{k})$ $+A_6(\underline{k})$	$-4B^*_{56}(-\underline{k})$	$-M_2-\lambda_{\underline{k}}$	$4B^*_{66}(\underline{k})$
$4B_{16}(\underline{k})$	$-2E_{16}(\underline{k})$ $A_2(\underline{k})$	$-4B_{26}(\underline{k})$	$2E^*_{26}(\underline{k})$ $+A^*_{12}(\underline{k})$	$4B_{36}(\underline{k})$	$-2E_{36}(\underline{k})$	$-4B_{46}(\underline{k})$	$2E^*_{46}(\underline{k})$	$4B_{56}(\underline{k})$	$-2E_{56}(\underline{k})$ $-A_6(\underline{k})$	$-4B_{66}(\underline{k})$	$M_2-\lambda_{\underline{k}}$

The numerical calculation of the dipole sums can be performed using the Ewald technique. This technique involves doing the sums to near atoms directly, and the sums for atoms at more than certain distance in reciprocal space (M. Born and K. Huang (1954)). The computer program for calculating these sums was written by Dr. E. R. Cowley of Brock University.

c - The effects of phenomenological anisotropy theory on the magnon dispersion curves of $CsMnF_3$:

At sufficiently low temperature ($T<<T_N$), the modulus of the sublattice magnetization vector $\underline{M}$ is practically independent of temperature and the anisotropy energy can be looked upon as a function only of direction of $\underline{M}$.

In the phenomenological description of an antiferromagnet the anisotropy Hamiltonian, H_{an}, is usually represented by an expansion in powers of the angular components of $\underline{M}$ and only the first few terms are retained (Landau and Lifshitz, 1960). The expansion must of course include only those combinations of the products of components of $\underline{M}$ which are invariant with respect to the symmetry elements of the crystal. These elements include the time reversal operation ($t \rightarrow -t$) in which the components of $\underline{M}$ change their signs. Consequently the expansion for H_{an} contains only even powers of the components of $\underline{M}$.

In actual fact we believe that most of the anisotropy

in $CsMnF_3$ arises from the dipole-dipole interactions. However since it has been widely used in the literature, we use the phenomenological single-ion anisotropy energies in this subsection and show the effect on the spin wave energies.

Microscopically for a simple two-sublattice uniaxial antiferromagnet one can write (Belson et al 1959) and (Smit et al 1959)

$$H_{an} = \sum_{\underline{R}} \frac{1}{2} [K_1(\cos^2\theta_1) + K_2(\cos^2\theta_2)] \qquad \text{(II-45)}$$

where K_1 and K_2 are the anisotropy constants and θ_1 and θ_2 are the angles between the direction of spins and the crystal symmetry axis. In the case where magnetic atoms in both sublattices have the same surrounding atoms; K_1 and K_2 are equal. We recall from the previous section that there is a large axial anisotropy along the c axis and a weak sixfold anisotropy in the basal plane of $CsMnF_3$. Thus ignoring the weak basal plane anisotropy, we can generalize the equation (II-45) and write

$$H_{an} = \sum_{\underline{R}} \frac{1}{6} \sum_{i=1}^{6} K_i \cos^2\theta_{i\underline{R}} \qquad \text{(II-46)}$$

Looking at the crystal symmetry of $CsMnF_3$ it can be shown that $K_1=K_4$ and $K_2=K_3=K_5=K_6$. Therefore there are two independent axial anisotropy constants K_1 and K_2. Since we have already assumed z (the equilibrium direction of the spin) to be the crystal (1,2,0) direction, the x component of the spin can be assumed to lie along the crystal c axis which is also the

direction of the effective fields. Then we can have $\cos\theta_i = S_i^x/S$, and consequently

$$H_{an} = \sum_{\underline{R}} \frac{1}{6} \{K_1 [(S^x_{1\underline{R}}/S)^2 + (S^x_{4\underline{R}}/S)^2] + K_2 [(S^x_{2\underline{R}}/S)^2 + (S^x_{3\underline{R}}/S)^2 + (S^x_{5\underline{R}}/S)^2 + (S^x_{6\underline{R}}/S)^2]\}. \quad \text{(II-47)}$$

Now we define the total sublattice magnetization, M, as

$$M = 3\ N\ S\ g\ \mu_B \quad \text{(II-48)}$$

where N is the number of cells in the specimen, g is the Landé factor, μ_B is the Bohr magneton and S is equal 5/2 for Mn^{2+} ion. Using equations (II-3), (II-27), (II-48) and going through some manipualtions H_{an} can be transformed to

$$\begin{aligned} H_{an} = E_0'' + \frac{\mu_B}{2} \{ & \frac{K_1}{M} [\sum_{\underline{R}} a_1^+ a_1^+ + a_1 a_1 + 2a_1^+ a_1 \\ & + a_4^+ a_4^+ + a_4 a_4 + 2a_4^+ a_4] \\ & + \frac{K_2}{M} [\sum_{\underline{R}} a_2^+ a_2^+ + a_2 a_2 + 2a_2^+ a_2 \\ & + a_3^+ a_3^+ + a_3 a_3 + 2a_3^+ a_3 \\ & + a_5^+ a_5^+ + a_5 a_5 + 2a_5^+ a_5 \\ & + a_6^+ a_6^+ + a_6 a_6 + 2a_6^+ a_6]\} . \end{aligned} \quad \text{(II-49)}$$

Note that $\frac{K_1}{M}$ and $\frac{K_2}{M}$ are the effective fields acting on the spins of Mn^{2+} ions. Using eq. (II-29) we write H_{an} in terms

of the spin wave operators $b(\underline{k})$ and $b^{+}(\underline{k})$,

$$
\begin{aligned}
H_{an} = E_0'' + \frac{\mu_B}{2} \{ & K_1/M[\sum_{\underline{k}} b_1^{+}(\underline{k}) b_1^{+}(-\underline{k}) + b_1(\underline{k}) b_1(-\underline{k}) \\
& + 2b_1^{+}(\underline{k}) b_1(\underline{k}) + b_4^{+}(\underline{k}) b_4^{+}(-\underline{k}) \\
& + b_4(\underline{k}) b_4(-\underline{k}) + 2b_4^{+}(\underline{k}) b_4(\underline{k})] \\
& + K_2/M[\sum_{\underline{k}} b_2^{+}(\underline{k}) b_2^{+}(-\underline{k}) + b_2(\underline{k}) b_2(-\underline{k}) \\
& + 2b_2^{+}(\underline{k}) b_2(\underline{k}) + b_3^{+}(\underline{k}) b_3^{+}(-\underline{k}) \\
& + b_3(\underline{k}) b_3(-\underline{k}) + 2b_3^{+}(\underline{k}) b_3(\underline{k}) \\
& + b_5^{+}(\underline{k}) b_5^{+}(-\underline{k}) + b_5(\underline{k}) b_5(-\underline{k}) \\
& + 2b_5^{+}(\underline{k}) b_5(\underline{k}) + b_6^{+}(\underline{k}) b_6^{+}(-\underline{k}) \\
& + b_6(\underline{k}) b_6(-\underline{k}) + 2b_6^{+}(\underline{k}) b_6(\underline{k})] \}.
\end{aligned}
\tag{II-50}
$$

Then recalling equation (II-30) the total Hamiltonian can be written as

$$
\begin{aligned}
H_T &= H_{ex} + H_{an} \\
&= E_0 + E_0'' + \sum_{\underline{k}} H_{ex}(\underline{k}) + \sum_{\underline{k}} H_{an}(\underline{k})
\end{aligned}
\tag{II-51}
$$

where E_0 is defined before and E_0'' is the constant term in H_{an}. Finally following the procedure we used to get from eq. (II-42) to (II-43) we get the following matrix equation which gives the eigenvalue $\lambda_{\underline{k}}$

$$
\begin{vmatrix}
M_1'-\lambda_{\underline{k}} & -D_1 & -A_2(\underline{k}) & 0 & 0 & 0 & 0 & 0 & 0 & 0 & -A_2^*(\underline{k}) & 0 \\
D_1 & -M_1'-\lambda_{\underline{k}} & 0 & A_2(\underline{k}) & 0 & 0 & 0 & 0 & 0 & 0 & 0 & A_2^*(\underline{k}) \\
A_2^*(\underline{k}) & 0 & -M_2'-\lambda_{\underline{k}} & D_2 & A_6^*(\underline{k}) & 0 & 0 & 0 & 0 & 0 & -A_{12}(\underline{k}) & 0 \\
0 & -A_2^*(\underline{k}) & -D_2 & M_2'-\lambda_{\underline{k}} & 0 & A_6^*(\underline{k}) & 0 & 0 & 0 & 0 & 0 & A_{12}(\underline{k}) \\
0 & 0 & -A_6(\underline{k}) & 0 & M_2'-\lambda_{\underline{k}} & -D_2 & -A_7(\underline{k}) & 0 & A_{11}(\underline{k}) & 0 & 0 & 0 \\
0 & 0 & 0 & A_6(\underline{k}) & D_2 & -M_2'-\lambda_{\underline{k}} & 0 & A_7(\underline{k}) & 0 & -A_{11}(\underline{k}) & 0 & 0 \\
0 & 0 & 0 & 0 & A_7^*(\underline{k}) & 0 & -M_1'-\lambda_{\underline{k}} & D_1 & A_7(\underline{k}) & 0 & 0 & 0 \\
0 & 0 & 0 & 0 & 0 & -A_7^*(\underline{k}) & -D_1 & M_1'-\lambda_{\underline{k}} & 0 & -A_7(\underline{k}) & 0 & 0 \\
0 & 0 & 0 & 0 & A_{11}^*(\underline{k}) & 0 & -A_7^*(\underline{k}) & 0 & M_2'-\lambda_{\underline{k}} & -D_2 & -A_6^*(\underline{k}) & 0 \\
0 & 0 & 0 & 0 & 0 & -A_{11}^*(\underline{k}) & 0 & A_7^*(\underline{k}) & D_2 & -M_2'-\lambda_{\underline{k}} & 0 & A_6^*(\underline{k}) \\
A_2(\underline{k}) & 0 & -A_{12}^*(\underline{k}) & 0 & 0 & 0 & 0 & 0 & A_6(\underline{k}) & 0 & -M_2'-\lambda_{\underline{k}} & D_2 \\
0 & -A_2(\underline{k}) & 0 & A_{12}^*(\underline{k}) & 0 & 0 & 0 & 0 & 0 & -A_6(\underline{k}) & -D_2 & M_2'-\lambda_{\underline{k}}
\end{vmatrix} = 0
$$

(II-52)

where $M_1'=2A_1+D_1$, $M_2'=A_1+A_4+A_{10}+D_2$, $D_1=-\frac{K_1}{M}\mu_B$ and $D_2=\frac{K_2}{M}\mu_B$. A_1 to A_{12} and K_1 and K_2 have been defined earlier. The eq. (II-52) can be solved numerically for any given wave vector $\underline{k}$ if the exchange constants and anisotropy constants are specified.

II-4 Interaction of Thermal Neutrons with Crystals:

The measurements of the phonons and magnons in solids can be done by various techniques, among which that of neutron scattering is the most important. A general account of neutron scattering techniques is given by P. A. Egelstaff (1965) and G. E. Bacon (1962). Here we will consider only the case of magnetic neutron scattering.

Since a neutron has a magnetic moment μ_N, its interaction with a magnetic field arising from the unpaired electrons of an atom can be written as (Marshall and Lovesey 1971)

$$-\sum_i \gamma\mu_N \hat{\underline{\sigma}} \cdot \underline{H}_i \qquad \text{(II-53)}$$

where the components of $\hat{\underline{\sigma}}$ are the Pauli spin matrices for the neutron and γ, the gyromagnetic ratio of neutron, is equal to 1.91. $\underline{H}_i$ is a magnetic field due to a single electron moving with velocity $\underline{V}_{ei}$ given by the Dirac's theory of the electron.

In the case where only the spin is scattering the neutron scattering cross-section of an N spin system per unit solid angle Ω and unit interval of outgoing energy E' can be written as (Marshall and Lovesey 1971)

$$\frac{d\sigma^2}{d\Omega dE'} = \left(\frac{\gamma e^2}{m_e c^2}\right) \frac{N}{\hbar} \frac{\underline{k}'}{\underline{k}} [f(\underline{Q})]^2 \tag{II-54}$$

$$\times \sum_{\alpha\beta} (\delta_{\alpha\beta} - \hat{Q}_\alpha \hat{Q}_\beta) S^{\alpha\beta}(\underline{Q},\omega)$$

where e and m_e are the charge and the mass of the electron and $f(\underline{Q})$ is the atomic form factor defined as the Fourier transform of the normalized spin density associated with the atom. $\underline{k}$ and $\underline{k}'$ are the incident and scattered wave vectors of the neutron. $\alpha,\beta = x,y,z$ and

$$S^{\alpha\beta}(\underline{Q},\omega) = \sum_{if} p_i \sum_{\ell\ell'} \exp(i\underline{Q}\cdot(\underline{R}_\ell - \underline{R}_{\ell'})) \tag{II-55}$$

$$\times \langle i|S^\alpha_\ell|f\rangle\langle f|S^\beta_{\ell'}|i\rangle \delta(\hbar\omega - E_i + E_f).$$

Here S^α_ℓ is the α component of the spin operator on the lattice site ℓ. $|i\rangle$ and $|f\rangle$ are the initial and final states of the spin system with E_i a nd E_f energies. P_i is the probability of finding target spin system in its initial state $|i\rangle$.

$$P_i = \frac{\exp(-E_i/K_B T)}{\sum_i \exp(-E_i/K_B T)} \tag{II-56}$$

where K_B is Boltzmann's constant and T is the absolute temperature.

Considering energy and momentum conservation laws, the change in the energy ($\hbar\omega$), and momentum ($\hbar\underline{Q}$) of the scattered neutron can be written as

$$\underline{Q} = \underline{k} - \underline{k}' = \underline{\tau} + \underline{q}$$
$$\hbar\omega = \frac{\hbar^2}{2M_n}(k^2 - k'^2) \quad . \tag{II-57}$$

$\underline{\tau}$ is a reciprocal lattice vector, and $\underline{q}$ is a vector in the first Brillouin zone of the target material. M_n is the neutron mass and, in eq. (II-54), $\hat{Q}_\alpha$ is the α direction cosine of $\underline{Q}$.

$S(\underline{Q},\omega)$ is the Van Hove's scattering function and is the space time Fourier transform of the time dependent spin-spin correlation function. It contains all the information about the scattering system.

It can be shown that for an isotropic Hamiltonian such as (II-12) eq. (II-54) reduces to (Marshall and Lovesey 1971)

$$\frac{d^2\sigma}{d\Omega dE'} = \left(\frac{\gamma e^2}{m_e c^2}\right)^2 \frac{N}{\hbar} \frac{\underline{k}'}{\underline{k}} |f(\underline{Q})|^2 (1+\hat{Q}_z^2) S^{xx}(\underline{Q},\omega)$$

where

$$S^{xx}(\underline{Q},\omega) = \sum_{if} p_i \sum_{\ell\ell'} \exp(i\underline{Q}\cdot(\underline{R}_\ell - \underline{R}_{\ell'})) \times \langle i|S_\ell^x|f\rangle\langle f|S_{\ell'}^x|i\rangle \delta(\hbar\omega + E_f - E_i) \quad . \tag{II-58}$$

Eq. (II-58) shows that the scattering cross section depends on the wave vector and energies of the incident and scattered particles, only. So the whole spin wave spectrum can be determined by means of neutron inelastic experiments.

For a simple antiferromagnet the magnetic dynamic structure factor (m.d.s.f.) is given by (Tondon 1973) and (Nagai

et al 1961)

$$\text{m.d.s.f.} = \cosh 2\theta_{\underline{q}} - \sinh 2\theta_{\underline{q}}(-1)$$

$$= (A_{\underline{q}} + B_{\underline{q}})/\lambda_{\underline{q}}$$

where $A_{\underline{q}}$, $B_{\underline{q}}$ and $\lambda_{\underline{q}}$ are defined in section (II-2).

Because of the complexity of the magnetism in $CsMnF_3$ the dynamic s.f.'s were not calculated and the experiment was carried out by simply looking for magnons in a number of different zones.

The nuclear elastic structure factor E_n is given by (Bacon 1962)

$$F_n(hk\ell) = \sum_j b_j \exp[2\pi i(hu_i + kv_i + \ell w_i)] \qquad \text{(II-59)}$$

where b_j is the scattering length of the atom j, h, k and ℓ are the Miller indices and u_j, v_j and w_j are the atomic coordinates of the jth atom in the cell.

Eq. (II-59) can be also used to calculate the magnetic elastic structure factor F_m, except that, instead of b_j one has to use the magnetic scattering amplitude p_j and sum over just the magnetic atoms (Bacon 1962). Using eq. (II-59) and proper nuclear and magnetic scattering amplitudes we calculated $I_n = |F_n|^2$ and $I_m = |F_m|^2$ for $CsMnF_3$. The results of the calculation are given in Table (II-1).

Table (II-1) Calculated nuclear and magnetic scattering intensities and the d spacings of some planes of $CsMnF_3$.

Miller Indices h	k	ℓ	d spacing A	I_n	I_m
0	0	1	15.074	0.000	0.219
0	0	2	7.537	0.176	0.000
0	0	3	5.025	0.000	60.686
0	0	4	3.768	0.137	0.000
0	0	5	3.015	0.000	6.802
0	0	6	2.512	245.705	0.000
0	0	7	2.153	0.000	5.626
0	0	8	1.884	0.104	0.000
0	0	9	1.599	0.233	-
1	0	0	5.381	0.003	0.000
2	0	0	2.690	0.060	0.000
3	0	0	1.794	1.283	0.000
4	0	0	1.345	0.864	0.000
5	0	0	1.076	0.615	0.000
6	0	0	0.897	106.151	0.000
7	0	0	0.768	0.001	0.000
8	0	0	0.673	8.678	0.000
9	0	0	0.598	2.128	-
1	0	1	5.067	1.081	14.082
2	0	1	2.648	26.876	13.195
4	0	1	1.341	28.880	11.269
2	2	0	1.553	132.642	0.000
2	0	2	2.534	61.202	14.666
4	0	2	1.324	50.918	12.595
2	0	3	2.372	73.607	0.008
4	0	3	1.299	70.149	0.001
2	0	4	2.189	32.333	6.015
2	2	6	1.321	223.655	0.000
2	0	8	1.543	36.404	16.119
2	0	9	1.422	38.041	0.837
2	1	1	2.015	7.314	10.301
3	1	1	1.485	1.300	10.217
1	0	2	4.379	1.335	16.218
2	1	2	1.963	1.991	11.572
3	0	3	1.687	2.026	42.585
1	1	3	2.642	0.000	37.425
1	0	7	1.999	0.787	24.473
1	0	8	1.778	1.760	43.482

CHAPTER III

EXPERIMENTAL APPARATUS AND TECHNIQUE

III-1 Specimens:

In order to study spin waves and magnetic critical phenomena in $CsMnF_3$ we used two different specimens. Details about these specimens are given separately in the next two paragraphs.

Specimen I: For spin wave studies we used a single crystal of $CsMnF_3$ which was purchased from Crystal Tec*. The crystal had a cylindrical shape of diameter 1.0 cm and length 4.5 cm. The directions of principal axes were determined by an x-ray precession camera. The crystal c axis was found to be 47.5 degrees from the cylindrical axis. Since we were interested in looking at the spin wave spectra in two major symmetry directions, the crystal was mounted with the (0 1 0) plane horizontal. Taking account of the spectrometer's resolution and using the maximum focussed neutron elastic peak, the mosaic spread of the specimen was estimated to be less than 8 minutes (Fig. III-1). A photograph of the crystal and its mount is given in Fig. (III-2) where the camera is looking at the direc-

---

*Crystal Tec
Centre d'Etudes Nucleaires des Grenoble,
Laboratoire d'Electronique et de Technologie de l'Informatique
Grenoble, France.

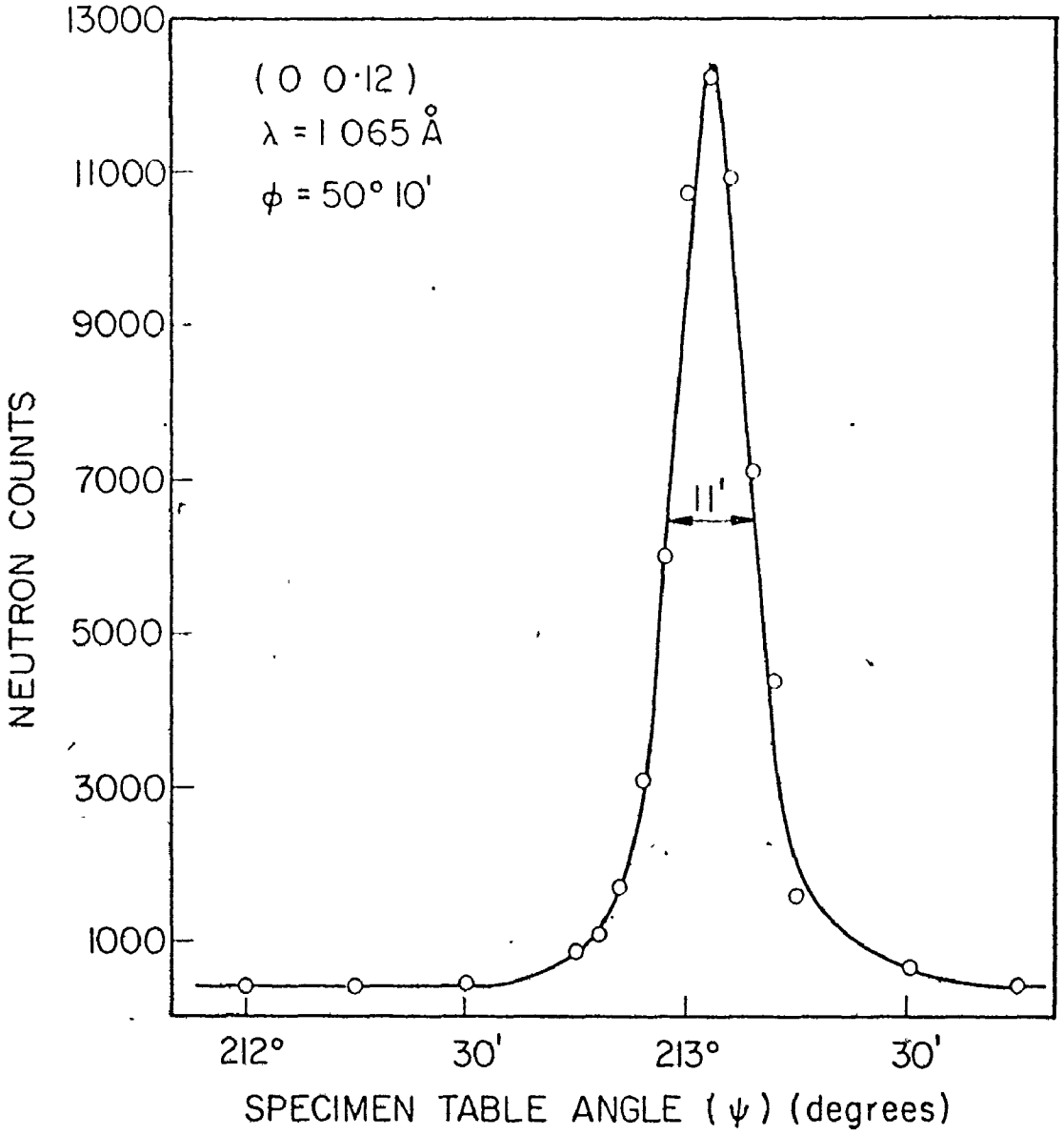

Fig. III-1 Maximum focussed neutron elastic peak (ψ scan) of the crystal.

Fig. III-2 Photograph of the crystal and its mount.

tion of the crystal a axis.

Specimen II: In order to avoid any extinction effects we used a powder specimen to measure the magnetic critical scattering. 30 grams of powdered $CsMnF_3$ was purchased from ICN K&K Labs*. The powder was placed in a tetragonal aluminum container of $4.5 \times 4.0 \times 0.5$ cm^3 size.

III-2 Cryostats:

Most parts of the experiment were carried out at liquid He temperature, and for this we used a cryostat which was made by Sulfrian Cryogenics†. Since the original sample chamber of the cryostat was too small for our work, we rebuilt the tail of the cryostat. The diameter of the new sample chamber is 5.5 cm. This cryostat holds liquid He for a period of 12 hours, so that for continuous experiments one has to refill every 12 hours. It is capable of keeping the temperature constant at 4.2 K, but is not equipped for varying the temperature.

For the last part of the experiment which a variable temperature cryostat was required, we purchased a cryostat from Oxford Instruments Inc.††. The tail of this cryostat was also designed and made at McMaster University. It has a cylindrical

---

*ICN Canada Ltd., 1956 Bourdon St., Montreal, Quebec H4M-1V1 Canada

†Sulfrian Cryogenics Inc., 391 East Inman Ave., Rahway, N.J. 07065, U.S.A.

††The Oxford Instrument Co. Ltd., Osney Mead, Oxford, England.

shape sample chamber with diameter 10 cm. This cryostat is insulated by super insulating material. Its liquid He capacity is 3 liters and holds liquid He for more than 24 hours. The temperature of the specimen can be controlled by varying the amount of current passing through the heater. The temperature range is 6 K to 78 K using liquid He and 78 K to room temperature using liquid N_2. With a good constant voltage power supplier the temperature stability is within 0.1°K.

We used two precalibrated GaAs diode thermometers for measuring the sample temperature. One of the thermometers was mounted on the top and the other on the bottom of the specimen so that it was possible to measure the temperature gradient across the sample. This temperature gradient was less than 0.1°K. The GaAs thermometers were purchased from Scientific Instruments Inc.*.

III-3 Measurements of Spin Waves:

Some preliminary experiments concerning the crystal structure of $CsMnF_3$ were carried out at the 2-axis spectrometer at the McMaster University reactor. Also a few points of the (1 0 0) acoustic branch of the magnon dispersion curves were measured by the 3-axis spectrometer at the McMaster University reactor.

---

*Scientific Instruments,Inc.
632 South F. Street/Lake Worth, Florida 33460 U.S.A.

All the other measurements described in this thesis were carried out on the McMaster University triple-axis spectrometer at the NRU Reactor of Chalk River Nuclear Laboratories. Detailed descriptions of this spectrometer have been given by Brockhouse (1961) and by Brockhouse et al (1968). A schematic diagram of this spectrometer is given in Fig. (III-3).

Neutrons of energy E_0 are selected from the continuous spectrum of the reactor by Bragg reflection from (2 2 0) planes of the Cu double monochromating crystals, with monochromating angle θ_m. This monochromatic beam of neutrons is scattered by the specimen through an angle ϕ into the analyzer, ψ being the orientation of the specimen with respect to incident beam. The scattered neutrons are detected by a He^3 counter at position B after Bragg reflection from the analyzing crystal, with an angle θ_A. The detector at position A acts as a background counter. The Soller collimators, C_2, C_3 and C_4 determine the directions of the neutrons. Collins (1963) and Cooper et al (1967) showed that the instrumental resolution depends on the collimation angles α_2, α_3 and α_4 of the individual collimators C_2, C_3 and C_4 respectively, and the mosaic spread of the monochromating and analyzing crystals.

It has been emphasized by Brockhouse (1961) that $\hbar Q$ (momentum transfer) and $\hbar\omega$ (energy transfer) are the natural variables for any neutron scattering experiments. Therefore it is natural to employ the "constant Q" or the "constant E"

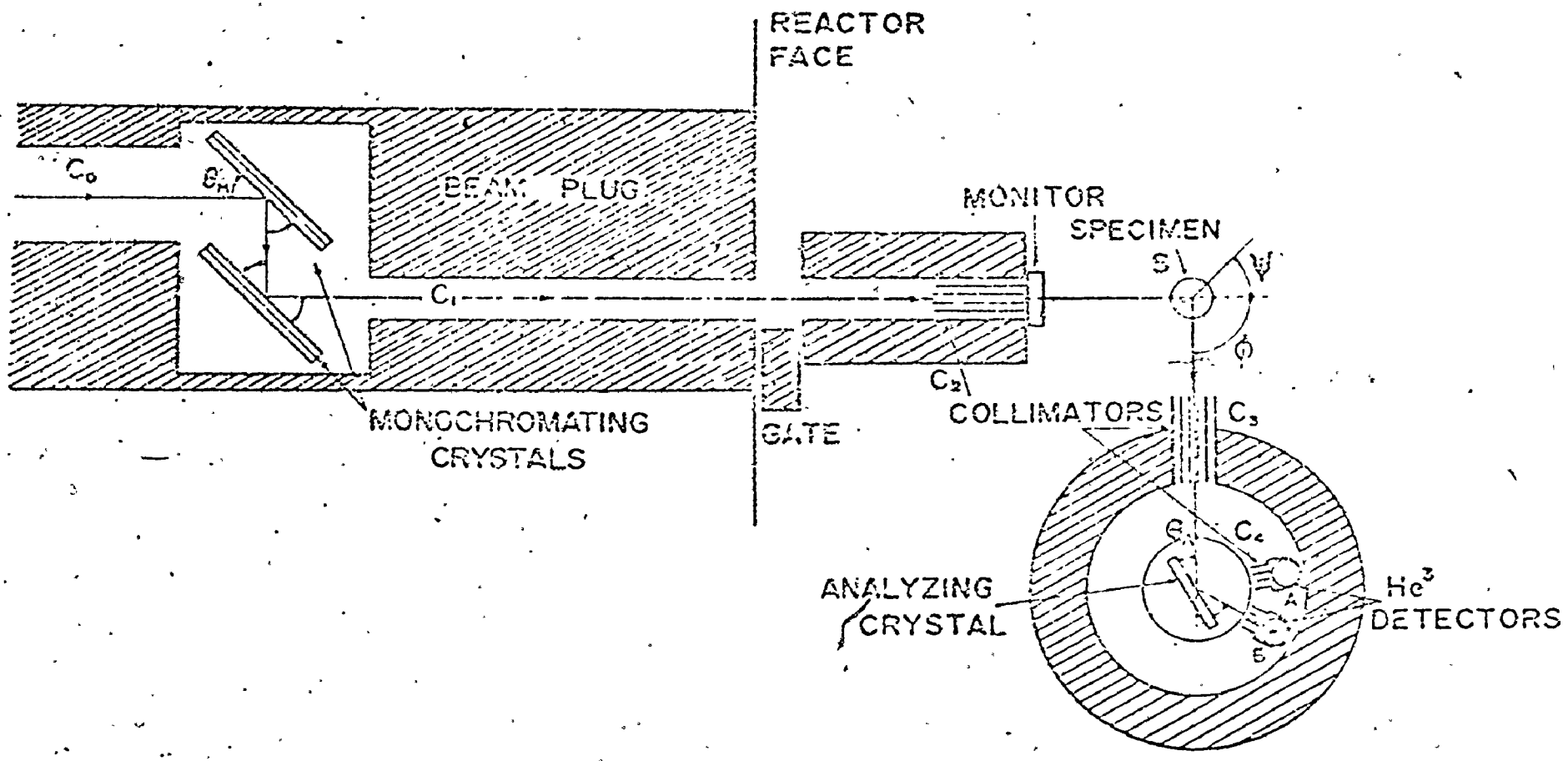

Fig. III-3 Schematic diagram of the McMaster (E2) triple-axis spectrometer at Chalk River.

method in the measurement of magnon spectra.

During an experiment, a major symmetry plane of the specimen is usually chosen to coincide with the spectrometer plane which is determined by the incident neutron wave vector $\underline{k}_0$ and scattered neutron wave vector $\underline{k}'$. ($\underline{k}_0$ was kept fixed throughout our experiments.) In the "constant Q" mode of operation, the experiments are performed by selecting a suitable $\underline{Q}$ to observe the magnon of interest and by scanning the range of frequency expected. Such a scan can be achieved by operating the spectrometer so that the values of ϕ, ψ and θ_A (or θ_m) are adjusted while keeping $\underline{Q}$ fixed. The operation is then controlled so as to record the number of counts at this particular point in the $(\underline{Q},\omega)$ space for a predetermined number of counts in the monitor fission detector and then to move three of the above angles so as to reach an adjacent point still keeping the value of $\underline{Q}$ unchanged. This process is repeated successively until the scanning of the predetermined frequency range is completed. The overall control of the machine is via preprogrammed punched tape produced by a computer. (For details of operation see Ph.D. thesis by A. Larose (1975).) After the scan, the frequency of the magnon of interest is determined by the peak of the neutron group, which occurs when the frequency and wave vector satisfy the dispersion relation. In the "constant E" mode of operation, the energy transfer is held fixed and $\underline{Q}$ is allowed to vary along some chosen direction in reciprocal space. The constant $\underline{Q}$ method is employed throughout these

experiments. Fig. (III-4) shows the photographs of the spectrometer with the Oxford cryostat on it.

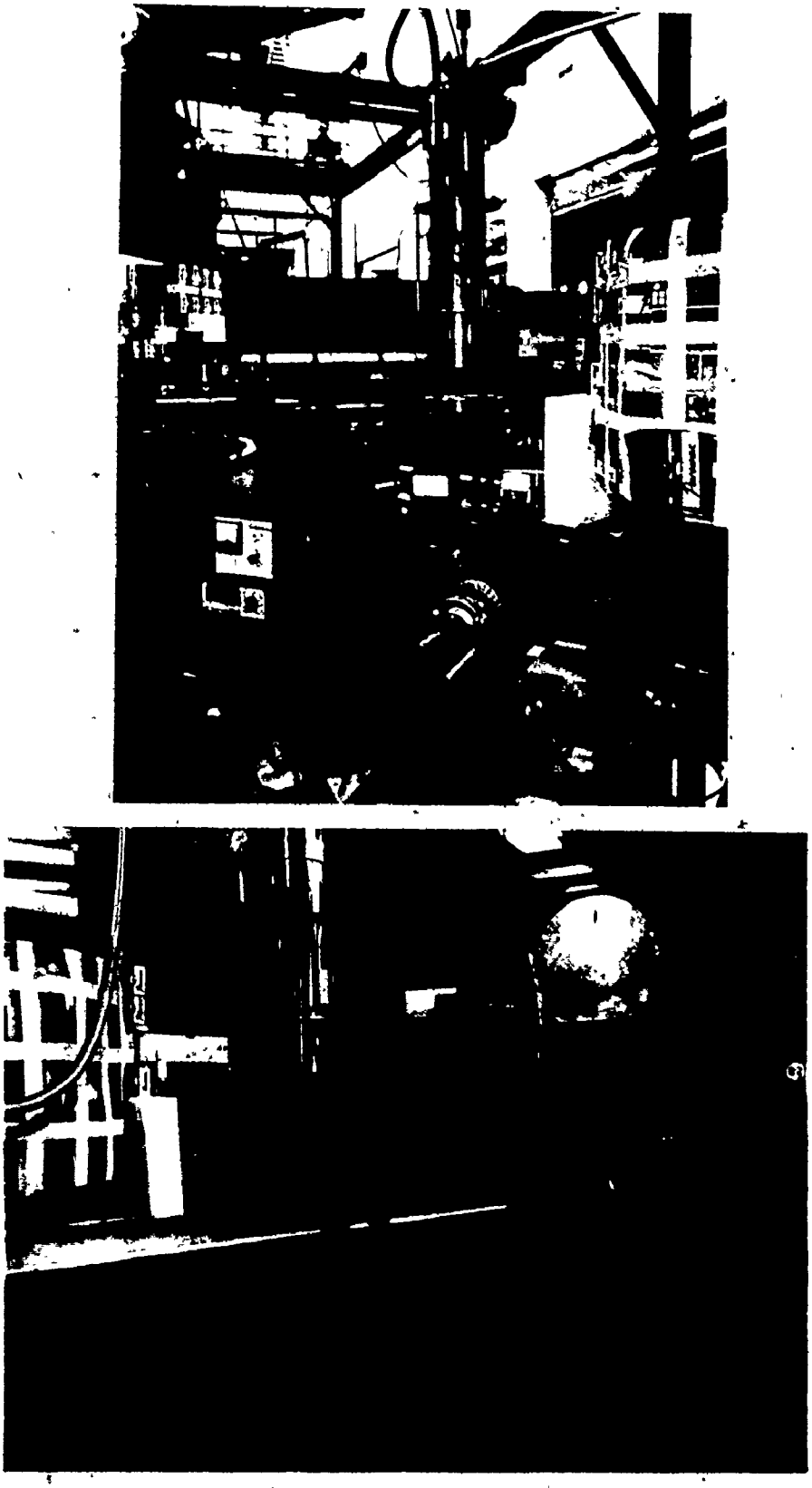

Fig. III-4 Two views of the triple-axis spectrometer at Chalk River with the Oxford cryostat on it.

CHAPTER IV

EXPERIMENTAL RESULTS AND DISCUSSION
PART I: SPIN WAVES

IV-1 General Remarks:

The magnon dispersion curves were obtained, by means of neutron inelastic scattering, along the two major symmetry directions, (00ξ) and (ξ00).

A few points of the (ξ00) acoustic branch were measured by the 3-axis spectrometer at the McMaster University reactor. Then we tried to measure some points of the (00ξ) acoustic branch and some points of the optic branches, but because of the low intensity we could not see any magnon peaks. Therefore the experiment was terminated at McMaster and continued on the McMaster triple-axis spectrometer at the NRU Reactor of Chalk River Nuclear Laboratories. At Chalk River, generally, the acoustic magnons were intense enough to be found easily, but the magnons of the optic branches only gave weak peaks. Since the dynamic structure factor was not calculated, many different zones were tried out and very long counting times were spent in order to obtain good counting statistics. Usually each scan took more than 12 hours and in some cases about 24 hours. All the magnon scans were carried out at 4.2 K initially, using the Sulfrian Cryostat (see section III-2). Except for the lower optic branch in the (ξ00) direction the

results were satisfactory at this temperature. After scanning for very long times and using many different zones, the magnons of the lower optic branch in the (ξ00) direction proved to be too weak to measure at 4.2 K. Therefore we transferred the specimen to the Oxford cryostat (see section III-2); raised the temperature to 18.2 K, and scanned again. This time the magnons were more intense and we were able to measure them. Later in this chapter we shall show how the results obtained at 18.2 K were normalized to 4.2 K.

In order to make sure that the results obtained at low temperatures were magnons rather than phonons or some other excitations, we repeated many of the scans at room temperature. The room temperature scans showed no peaks and proved that indeed our low temperature peaks were magnons.

In order to have good energy resolution for measuring the acoustic magnons, we selected an incident neutron beam of frequency 3.849 THz. (This is the lower limit of the McMaster 3-axis spectrometer at the Chalk River NRU Reactor.) It should be mentioned that the intensity of the beam at this frequency is low. Thus for looking at the optic branches we needed a beam with more intensity. To obtain a more intense beam we sacrificed resolution and selected an incident neutron beam of frequency 6.538 THz. This lies almost in the middle of the reactor spectrum, and the number of neutrons available at this frequency is the highest obtainable.

IV-2 Method of Analyzing Data:

The experimental results were plotted and the data points seemed to give complete dispersion curves in the two high symmetry directions. Thus we developed a theory of spin waves for $CsMnF_3$ (see section II-3) and attempted to fit it to the observed results. A specific direction was assumed for the spins and the dipole sums, given in eq. (II-44), were calculated. Then by using the results of the dipole sums and varying the three exchange constants, the matrix equation (II-43) was fitted to the experimental results. The results of calculations were satisfactory and identical for all the directions in the basal plane of the crystal. But when the spins were assumed to be aligned along the c axis, the calculated spin wave frequencies came out to be complex numbers. Also some other directions, out of the basal plane, were tried and the results showed that the spin system goes unstable.

In order to obtain a least-squares fit to data, a function F was defined by

$$F = \frac{1}{N-M} \sum_{n=1}^{N} \left[\frac{\nu_c(n)-\nu_{exp}(n)}{\Delta\nu_{exp}(n)}\right]^2 \qquad \text{(IV-1)}$$

where N is the number of data points, M is the number of adjustable parameters (in this case the three independent exchange constants J_{12}, J_{23} and J_{35}), $\nu_c(n)$ is the calculated magnon frequency, $\nu_{exp}(n)$ is the observed frequency and $\Delta\nu_{exp}(n)$ is the estimated error on the determination of the observed magnon frequency. The function F was minimized, giving a minimum

value of $F_{min} = 0.91$. The optimum values of the exchange constants, corresponding to this minimum, were determined. For later use we denote the optimum fitted exchange constants by J_{12}^0, J_{23}^0 and J_{35}^0.

To estimate the error in each of the three exchange constants, we proceeded in the following way. First F_{min} was normalized to 1 and six different values for F were calculated. F_1 was calculated by having $J_{12} = J_{12}^0 + \Delta J_{12}^0$, $J_{23} = J_{23}^0$ and $J_{35} = J_{35}^0$. F_2 and F_3 were obtained in the same way except that, instead of J_{12}, J_{23} and J_{35} were in turn increased by ΔJ_{23}^0 and ΔJ_{35}^0. F_4 was calculated with $J_{12} = J_{12}^0 + \Delta J_{12}^0$, $J_{23} = J_{23}^0 + \Delta J_{23}^0$ and $J_{35} = J_{35}^0$. F_5 and F_6 were also obtained in the same way as F_4 except that, instead of J_{35}, J_{23} and J_{12} were kept at their optimum values respectively. In this calculation we had $\Delta J_{12}^0 = J_{12}^0/100$, $\Delta J_{23}^0 = J_{23}^0/100$ and $\Delta J_{35}^0 = J_{35}^0/20$. Then to a first approximation we assumed the function ΔF (deviation of F from its minimum value) to have the quadratic form

$$\begin{aligned}\Delta F &= F-1 \\ &= A_1(\Delta J_{12})^2 + A_2(\Delta J_{23})^2 + A_3(\Delta J_{35})^2 \\ &\quad + 2[A_4(\Delta J_{12})(\Delta J_{23}) + A_5(\Delta J_{12})(\Delta J_{35}) \\ &\quad + A_6(\Delta J_{23})(\Delta J_{35})]\end{aligned} \qquad \text{(IV-2)}$$

for small values of ΔJ_{12}, ΔJ_{23} and ΔJ_{35}. A_1 to A_6 are the coefficients of the quadratic equation and ΔJ_{12}, ΔJ_{23} and ΔJ_{35} are the deviations of J_{12}, J_{23} and J_{35} from their optimum

values. Using equation (IV-2), F_1 to F_6 and the values of ΔJ's, A_1 to A_6 were calculated for two standard errors in F. Then the principle axes of the ellipsoid and their directions were determined by diagonalizing and getting the eigen vectors of the matrix

$$\begin{pmatrix} A_1 & A_4 & A_5 \\ A_4 & A_2 & A_6 \\ A_5 & A_6 & A_3 \end{pmatrix}$$

We denote the eigenvalues by DA_1, DA_2 and DA_3. The eigen vectors showed that J_{23} was almost independent of J_{12} and J_{35}, but J_{12} and J_{35} were correlated. So the error in J_{23} was simply obtained by inverting and taking the square root of DA_2. In order to estimate the errors in J_{12} and J_{35} we followed a similar procedure as for J_{23}, which also took account of the correlation effects.

IV-3 General Description of the Results:

As it was mentioned in section (III-3), the constant Q method was used throughout these experiments. Therefore each magnon was identified with a given value of Q and provided us with raw data consisting of the neutron counts versus the neutron frequency loss. The raw data were plotted and the magnon creation peaks were obtained (of course in cases where there was a peak!). Then each peak frequency was determined

carefully and, according to the goodness of the peak, an estimated error was assigned to the peak frequency. Some of these magnon peaks are shown in figures (IV-1), (IV-2) and (IV-3), where the small circles represent the observed data points and the solid curves are drawn by hand. The figures show that, while the low $\underline{q}$ acoustic peaks are very sharp and well defined, the others, in general, are broad. For the broad peaks, errors of 0.02, 0.03 and even in some rare cases 0.04 THz were given.

The magnon frequencies of the lower optic ($\xi 00$) branch were obtained at 18.2 K. Therefore a small correction had to be made to map these frequencies back to 4.2 K, where the rest of the dispersion curves were determined. To do this we assumed that the magnon frequencies in $CsMnF_3$ would approximately have the same temperature and $\underline{q}$ dependence as in $RbMnF_3$ and used the experimental results of Saunderson et al (1972), which gives the temperature and wave vector dependence of spin wave energies in $RbMnF_3$. The changes in mean frequency with increasing temperature are given in figure (IV-4) as fractional shifts,

$$\frac{\Delta\nu(T)}{\nu(4.2)} = \frac{\nu(4.2)-\nu(T)}{\nu(4.2)}$$

versus reduced wave vector, $q^* = a|\underline{q}|/\pi$, where $\nu(4.2)$ is the frequency at the corresponding q^* from a smoothed, two-parameter, fitted dispersion relation to the 4.2 K data. According to this figure spin waves in $RbMnF_3$ are softened independent of wave vector by 2.8%, when the temperature is raised from

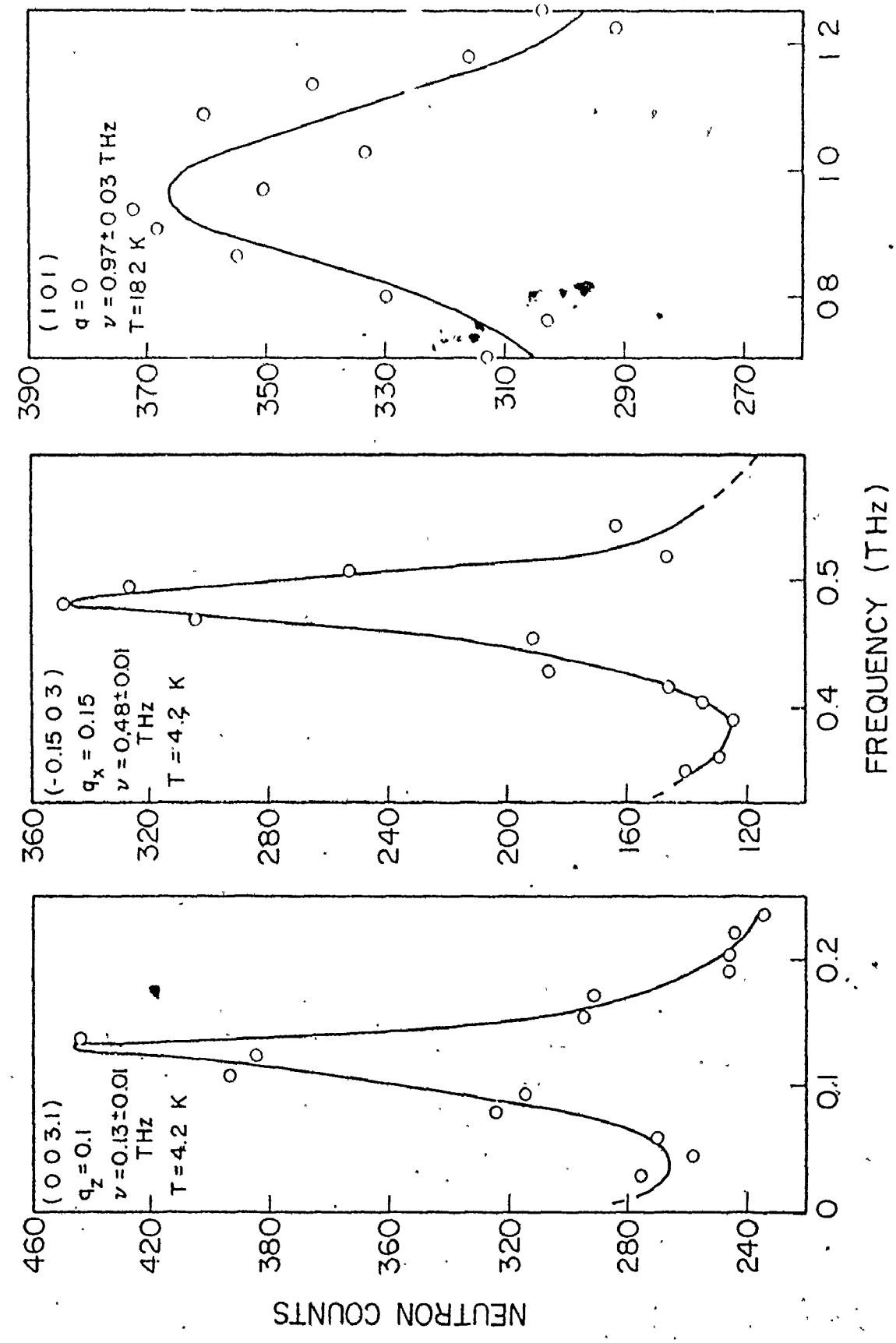

Fig. IV-1 Three of the magnon creation peaks in $CsMnF_3$. The solid curves are drawn by hand.

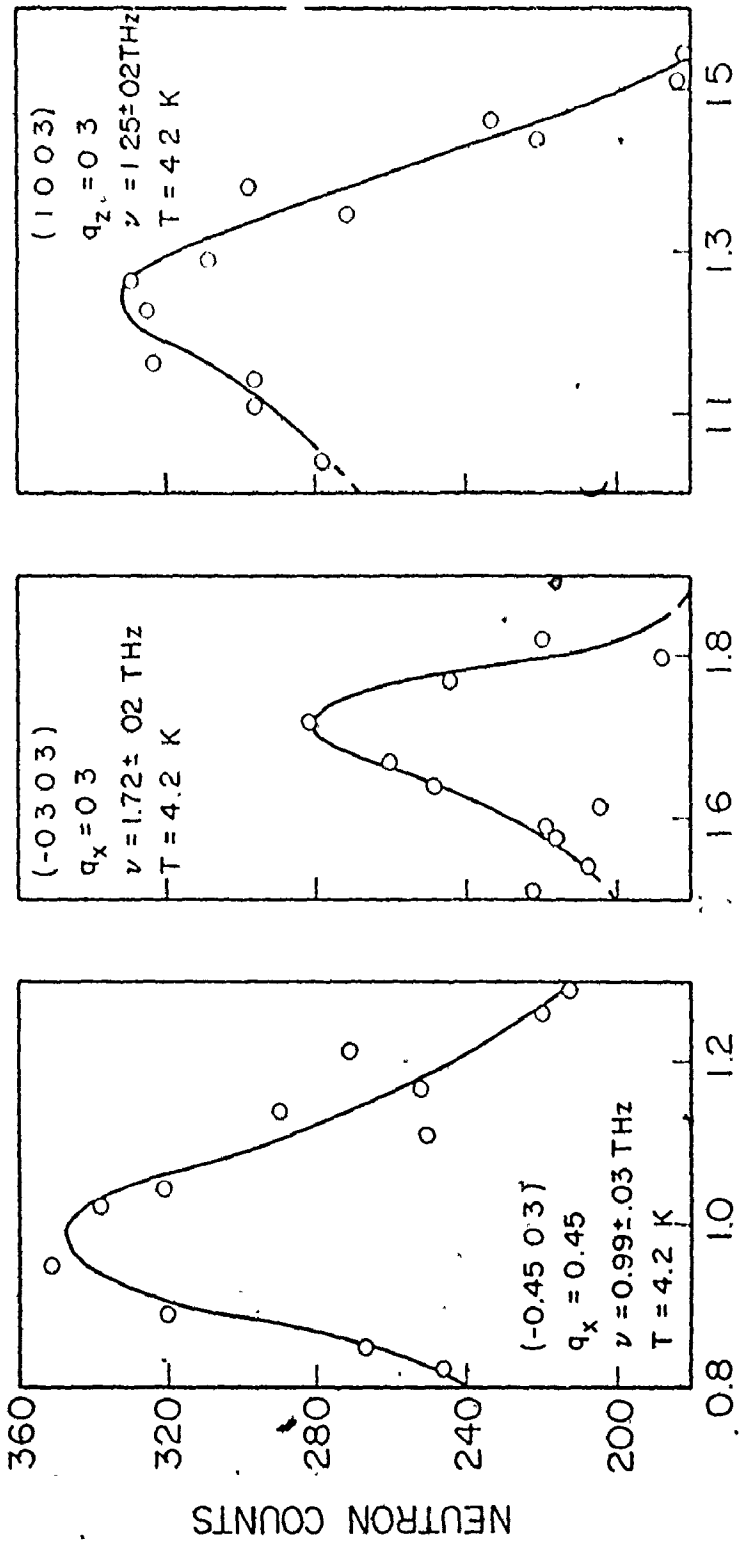

Fig. IV-2 Three of the magnon creation peaks in $CsMnF_3$. The solid curves are drawn by hand.

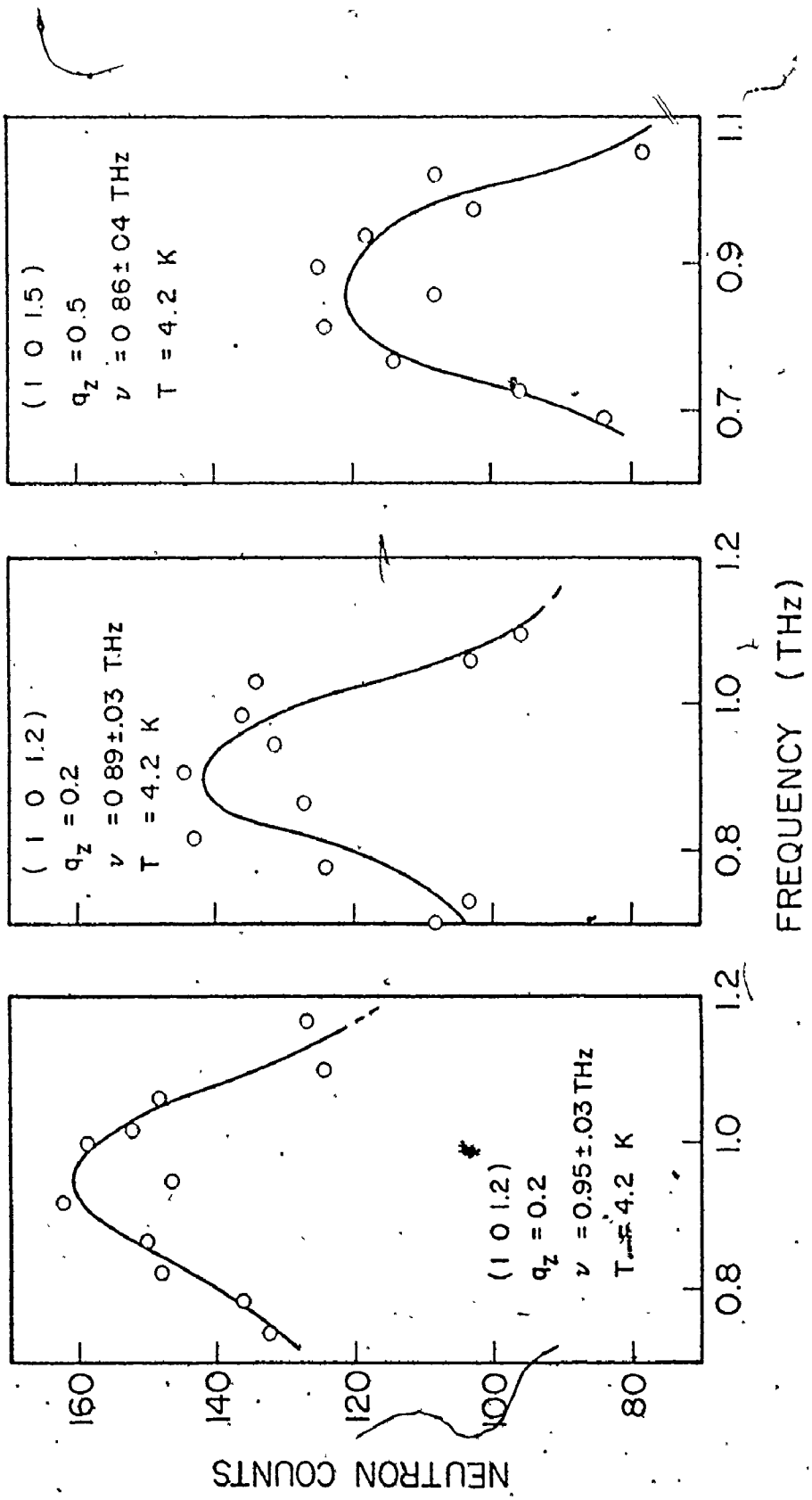

Fig. IV-3 Three of the magnon creation peaks in $CsMnF_3$. The solid curves are drawn by hand.

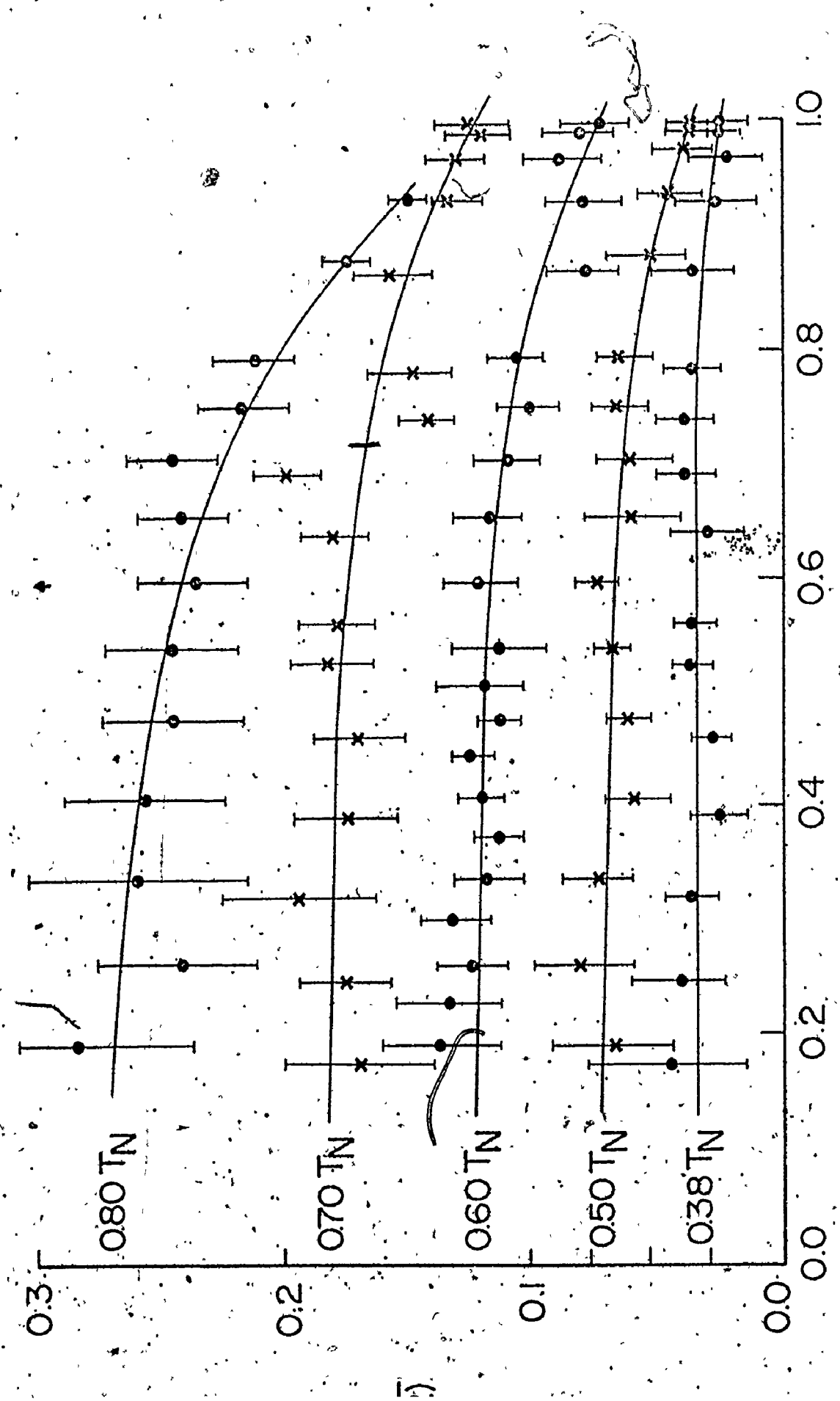

Fig. IV-4 Fractional mean frequency shifts of spin waves in $RbMnF_3$. Lines are given by the two parameter model fitted to the neutron data at each temperature.

4.2 K to 0.38 T_N. In our case the temperature of the sample was raised from 4.2 K to 18.2 K (0.36 T_N); the equivalent correction would be 2.5%. This correction is very small and in some cases is even smaller than the estimated error in the spin wave frequency. The observed magnon frequencies for each $\underline{q}$ value, at 4.2 K, are given in table (IV-1). Also table (IV-1) includes the estimated error of each of these frequencies.

The complete magnon dispersion curves are shown in figures (IV-5) and (IV-6). The small circles with the error bars are the observed data points and the solid curves are obtained from the theory given in section (II-3-b). These figures show that most of the experimental points lie on the theoretical curves, and the overall fit is quite satisfactory. It follows that the spin-wave excitations are well represented by our theoretical model, and that our starting Hamiltonian is a good description of the magnetic properties of $CsMnF_3$.

IV-4: The Exchange Constants:

The best fit to the observed data points is shown in figures (IV-5) and (IV-6) by the solid curves. The optimum values for the exchange constants were determined to be:

$$J_{12} = 0.134 \pm .003 \text{ THz} \quad , \quad J_{23} = 0.094 \pm .0105 \text{ THz.}$$

and

$$J_{35} = -0.0138 \pm .003 \text{ THz.}$$

Seavey et al (1969), using parallel pumping technique, ob-

Table (IV-1) Magnon frequencies (in units of THz) of $CsMnF_3$ at 4.2 K with estimated errors.

(00ξ) Branch			
$\xi=cq_z/2\pi$	ν_1 (Acoustic)	ν_2 (Optic)	ν_3 (Optic)
0.10	0.132 ±.01	-	1.24 ±.03
0.15	0.155 ±.02	-	-
0.20	0.215 ±.02	0.95 ±.03	1.25 ±.02
0.25	0.255 ±.02	-	-
0.30	0.25 ±.03	0.89 ±.03	1.255 ±.02
0.35	0.34 ±.03	-	-
0.40	0.31 ±.03	0.88 ±.03	1.28 ±.03
0.45	0.35 ±.03	-	-
0.50	0.38 ±.02	0.86 ±.04	1.28 ±.03
(ξ00) Branch			
$\xi=aq_x/2\pi$	ν_1 (Acoustic)	ν_2 (Optic)	ν_3 (Optic)
0.00	-	0.99 ±.03	1.17 ±.03
0.05	0.156 ±.01	-	1.26 ±.03
0.10	0.312 ±.01	1.05 ±.02	1.35 ±.03
0.15	0.483 ±.01	-	1.42 ±.02
0.20	0.62 ±.02	1.08 ±.03	1.45 ±.03
0.25	0.77 ±.02	-	1.57 ±.03
0.30	0.89 ±.03	1.11 ±.03	1.72 ±.02
0.35	0.98 ±.02	-	1.91 ±.03
0.40	1.02 ±.03	1.11 ±.03	1.87 ±.03
			1.94 04

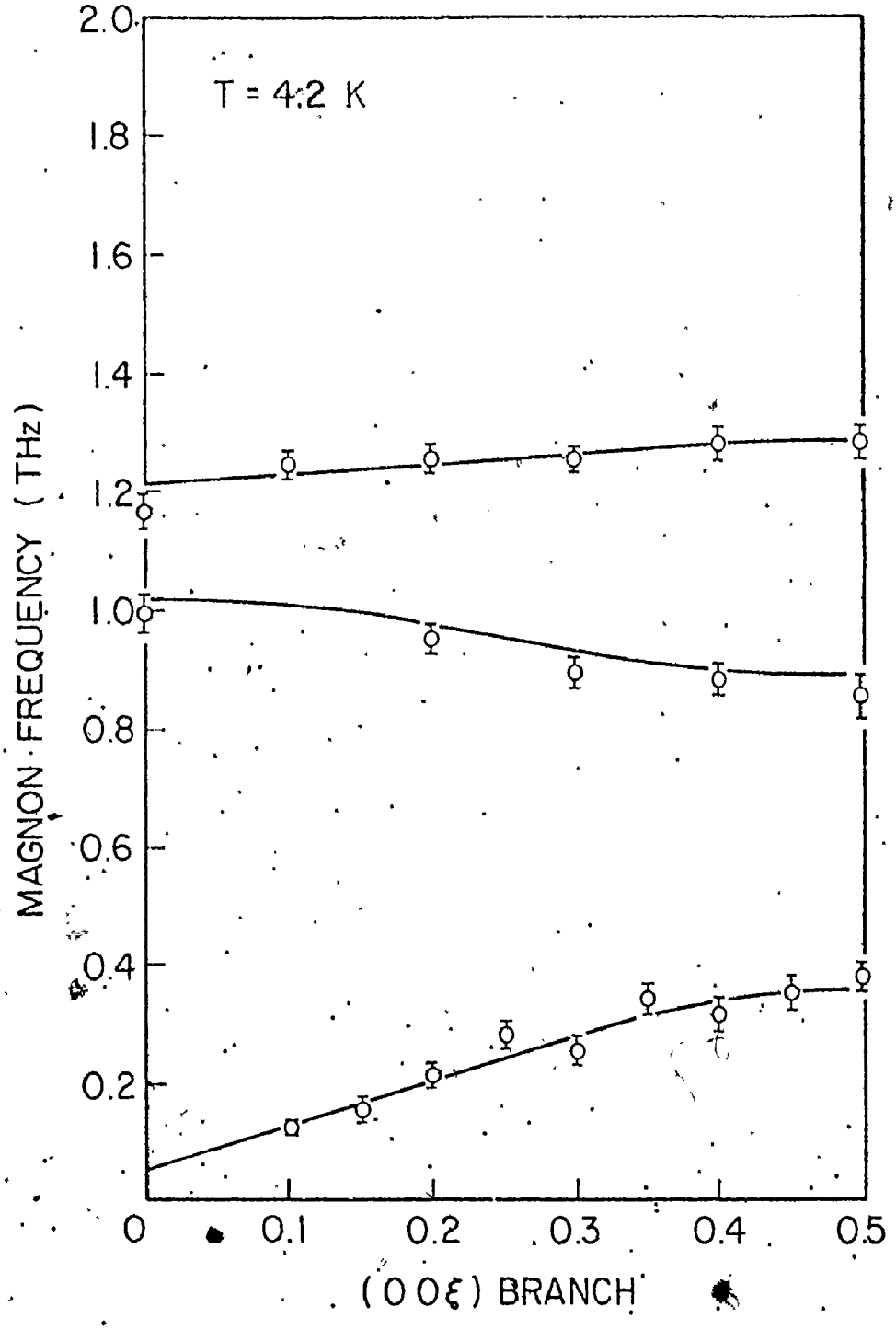

Fig. IV-5 Magnon dispersion curves of $CsMnF_3$ along the (00ξ) direction. The small circles with the error bars are the observed data points and the solid curves represent the best fit to the data.

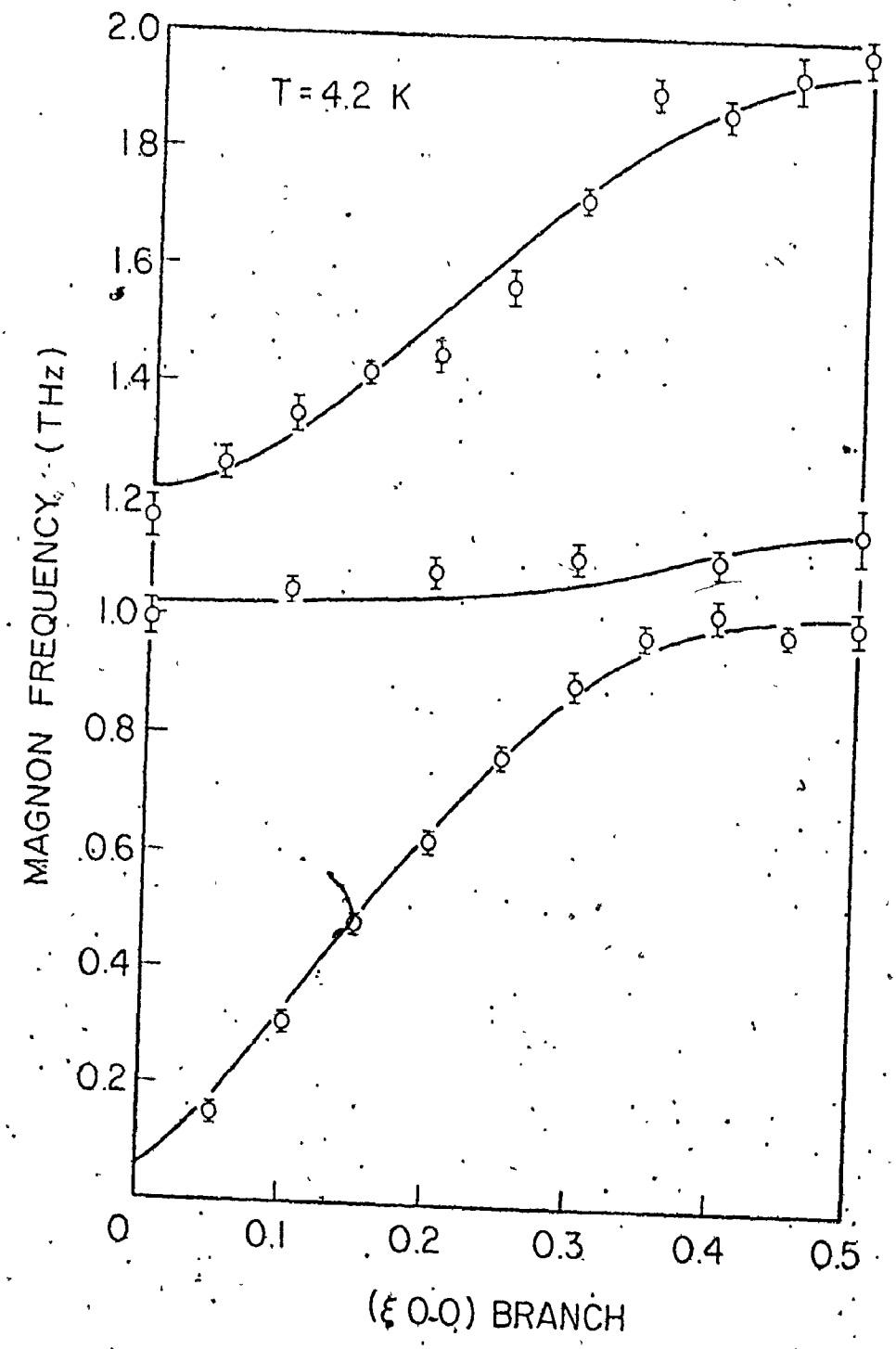

Fig. IV-6 Magnon dispersion curves for $CsMnF_3$ along the (ξ0,0) direction. The small circles with the error bars are the observed data points and the solid curves represent the to

tained the values 0.105 THz and 0.096 THz for J_{12} and J_{23} respectively. However, they assumed just two non zero exchange constants, J_{12} and J_{23}, which does not satisfy our observations. This can be seen in figures (IV-7) and (IV-8), where the solid curves, representing the theory with $J_{35} = 0$, are compared with the experimental data points.

IV-5 Anisotropy Fields:

Assuming just dipole-dipole interactions as the source of anisotropy, our results indicate that there is a negative axial anisotropy field, which forces the spins to stay on the basal plane and no anisotropy in the plane. In this section we shall attempt to calculate the magnitude of this axial anisotropy field.

The effective anisotropy fields, K_1/M and K_2/M, were defined in section (II-3-c). Note that K_1/M and K_2/M are assumed to be along the crystal c axis and the spins are constrained to the basal plane. Also it is worth recalling that, K_1/M acts on the spins of Mn_1 and Mn_4 atoms and K_2/M acts on the spins of Mn_2, Mn_3, Mn_5 and Mn_6 atoms.

Since the inclusion of the effective anisotropy field in the spin wave theory affects, mainly, the magnon frequencies at $q = 0$, we calculated the magnon frequencies at $q = 0$ for several K_1/M and K_2/M values and compared the results with the values shown in figures (IV-5) and (IV-6). Through this procedure we found that, the only satisfactory result can be

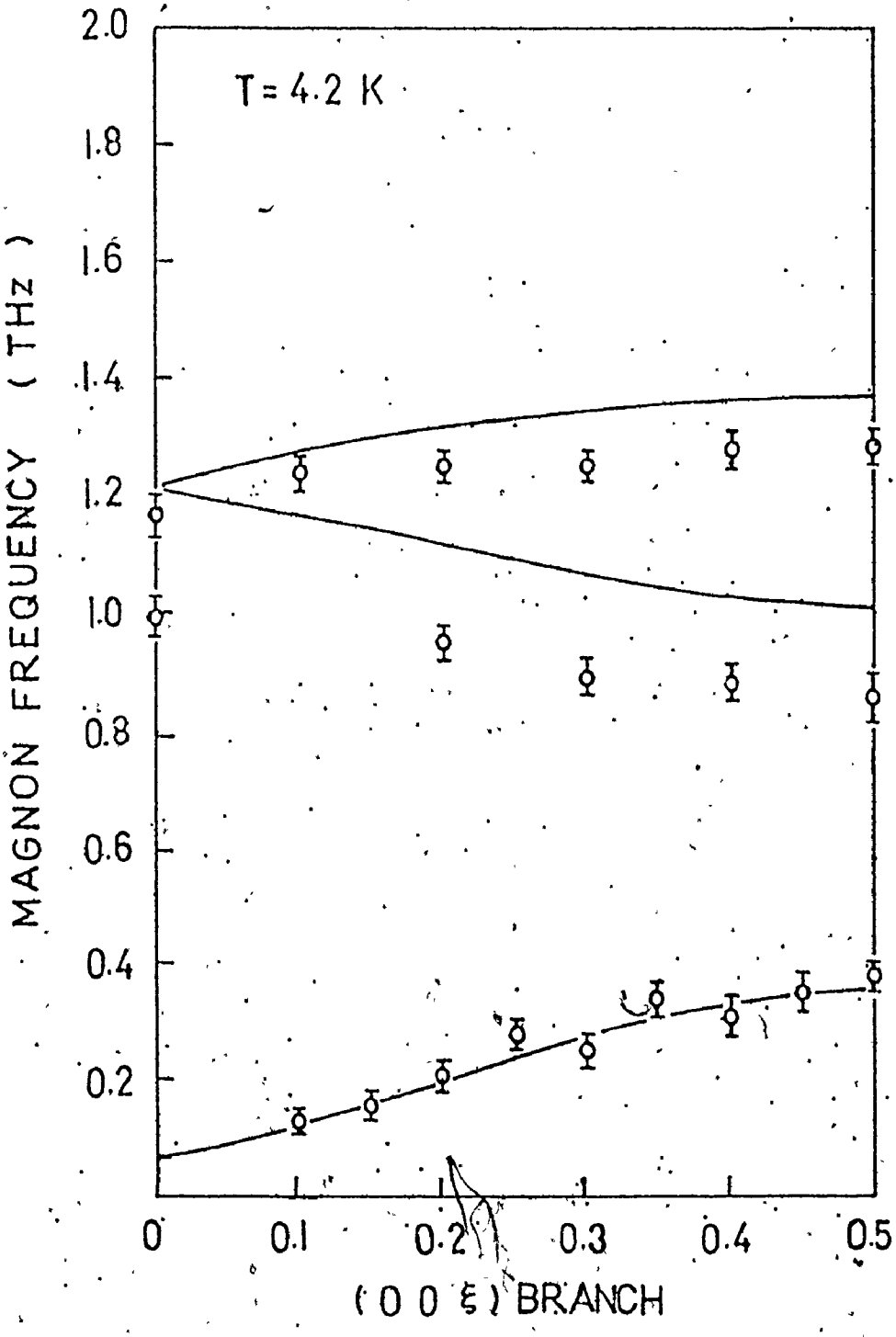

Fig. IV-7 . Magnon dispersion curves of $CsMnF_3$ along the (00ξ) direction. The solid curves, representing the theory with only two

are

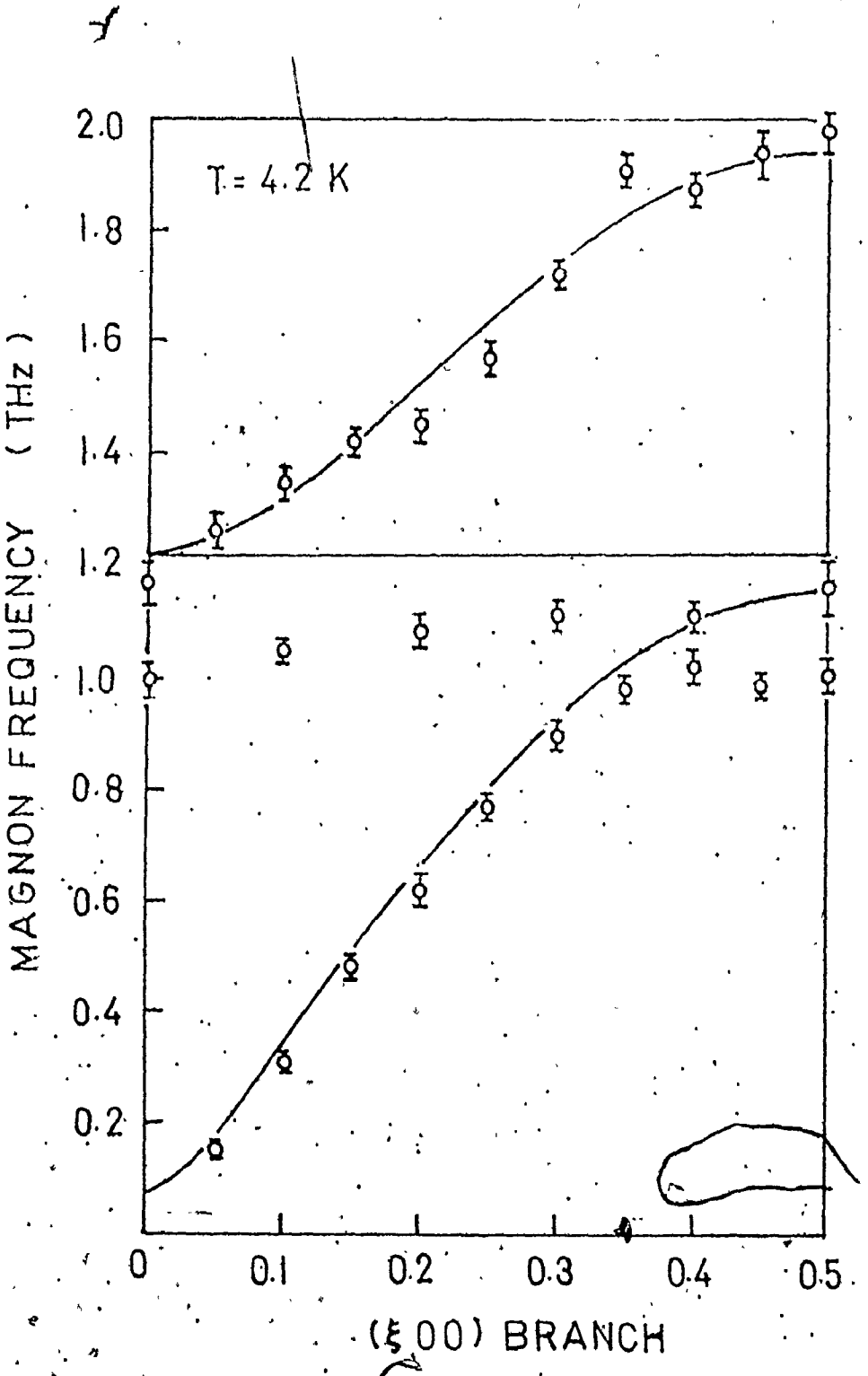

Fig. IV-8 Magnon dispersion curves of $CsMnF_3$ along the (ξ00) direction. The solid curves, representing the theory with only two nearest neighbour exchange constants, are

obtained by putting

$$K_1/M = K_2/M = -2700 \pm 900 \text{ Oe.}$$

The fact that $K_1/M = K_2/M$ agrees with the results of K. Lee et al (1963), but the value 2700 Oe is much smaller than their result, 7500 Oe. Assuming an anisotropy field of -7500 Oe, and q = 0 we get 0.2 THz for the acoustic magnon frequency. As figures (IV-5) and (IV-6) show, 0.2 THz is much larger than the value we obtained experimentally.

CHAPTER V

EXPERIMENTAL RESULTS AND DISCUSSION PART II: CRITICAL MAGNETIC SCATTERING

V-1 General Remarks:

In this chapter we shall report the results of magnetic neutron scattering from a powder specimen of $CsMnF_3$ and shall use them to find the critical index β.

Using equation (II-51) one can show (de Gennes 1963) that

$$I \sim M^2(T) \qquad (V-1)$$

where I is the elastic (or Bragg) magnetic scattering intensity and M(T) is the spontaneous magnetization at temperature T. Then from equations (V-1) and (I-2) one gets

$$I \sim M^2(T) \sim (1 - T/T_c)^{2\beta} \qquad (V-2)$$

which leads to a way of measuring the exponent β. Equation (V-2) should hold for an anisotropic antiferromagnet realizing that M(T) is the spontaneous sublattice magnetization.

In order to measure M(T) as accurately as possible, it is desirable to find a scattering plane with a large magnetic scattering intensity and zero (or very low) nuclear scattering intensity. Inspection of table (II-1) and our previous experimental results from single crystal of $CsMnF_3$

shows that the (003) and (101) planes both have a very small nuclear scattering intensity and high magnetic scattering intensity. Table (II-1) also shows that the d spacings of (003) and (101) planes are very close to each other. This made us suspect that using a powder specimen to measure either of these peaks might result in difficulties. The primary reason for using a powder sample was to eliminate extinction effects. In this experiment we used a neutron beam of 1.317 Å which gave a separation of about 0.1 degrees betwen the (003) and (101) peaks. This separation is too small to be resolved with our instrument and it is also very small in comparison with the full half height width (FHHW) of the powder patterns. Thus we realized that the powder specimen does not cause any difficulty because the two peaks simply lie on top of each other. In fact having the two peaks together adds to the intensity of the magnetic peak and provides better statistics. This is confirmed by figure (V-1) which gives the powder pattern of (003) plus (101) at 6.8 K and 295 K. The flatness of the powder pattern at 295 K indicates that the nuclear intensity of (003) plus (101) is practically zero.

The Oxford cryostat (section II-2) was used in this experiment. During each count the temperature of the sample was controlled manually and kept constant within 0.1°K. Also the temperature gradient across the sample was measured several times and was found to be less than 0.1°K.

V-2 Experimental Results:

The complete powder pattern of the specimen was taken with the double axis spectrometer at the McMaster University nuclear reactor. All the peaks belonging to $CsMnF_3$ and Al (the sample container) were present. This showed that the sample was indeed $CsMnF_3$ with a high purity factor. All the other results reported here were taken with the McMaster triple-axis spectrometer at the NRU Reactor of Chalk River Nuclear Laboratories. The analyser crystal of the spectrometer was set so that the counter would detect only the elastically scattered neutrons. The beam had a wave length of 1.317 Å and, as the room temperature measurements of figure (V-1) shows, the half wave length contamination was very small.

The superimposed (101) and (003) peak position was found at 6.8 K and the counter angle was maintained at the peak position for the rest of the experiment. The temperature of the specimen was raised stepwise and at each step maintained constant while the peak intensity was measured. After every few temperature steps the powder pattern of the peak was taken to see whether the peak profile had changed in any way. Three of these powder patterns are shown in figures (V-1) and (V-2). These powder patterns were taken at 6.8 K, 33.3 K and 47.2 K. They show that, the width (FHHW) stayed constant at 36' and the peak position changed only by 0.1

V-2 Experimental Results:

The complete powder pattern of the specimen was taken with the double axis spectrometer at the McMaster University nuclear reactor. All the peaks belonging to $CsMnF_3$ and Al (the sample container) were present. This showed that the sample was indeed $CsMnF_3$ with a high purity factor. All the other results reported here were taken with the McMaster triple-axis spectrometer at the NRU Reactor of Chalk River Nuclear Laboratories. The analyser crystal of the spectrometer was set so that the counter would detect only the elastically scattered neutrons. The beam had a wave length of 1.317 Å and, as the room temperature measurements of figure (V-1) shows, the half wave length contamination was very small.

The superimposed (101) and (003) peak position was found at 6.8 K and the counter angle was maintained at the peak position for the rest of the experiment. The temperature of the specimen was raised stepwise and at each step maintained constant while the peak intensity was measured. After every few temperature steps the powder pattern of the peak was taken to see whether the peak profile had changed in any way. Three of these powder patterns are shown in figures (V-1) and (V-2). These powder patterns were taken at 6.8 K, 33.3 K and 47.2 K. They show that, the width (FHHW) stayed constant at 36' and the peak position changed only by 0.1

degrees; to correct for this in taking measurements at intermediate temperatures the counter angle was adjusted. They also show that the wing intensity (background) increases with temperature. Therefore a corresponding background was assigned to each peak. The experimental data are given in table (V-1). Near T_c each count was over a period of 2 hours and far from T_c, each count was over a period of 30 minutes. In table (V-1) each count and the estimated background has been normalized to 1.5 hours which amounts to 300,000 monitor counts.

In figure (V-3) we have plotted the peak intensity versus temperature. The small circles represent the observed intensity and the solid line is drawn by hand. This shows that the peak intensity varies smoothly with temperature and behaves qualitatively just as would be expected for a critical phase transition at about 50 K.

V-3 Critical Exponent β:

Considering equation (V-2) one can write

$$\beta = \frac{1}{2} \frac{\text{Log } I}{\text{Log}(1-T/T_c)}$$

where I = peak intensity-background. Thus the critical exponent of the magnetization β can be obtained directly from the log-log plot of I versus $(1-T/T_c)$ if the critical temperature is specified.

Since T_c is not accurately known, four possible values for T_c were considered, 49.5, 49.6, 49.7 and 49.8 K. In log-

Table (V-1) Observed (101)+(003) magnetic peak intensity and corresponding estimated background versus temperature

Temperature degrees K	Counts/1.5 hours	Estimated Background
6.8	38020	2400
13.7	36097	2550
21.4	33045	2750
28.25	29392	3000
33.5	26250	3300
33.9	26197	3300
38.65	21816	3700
42.75	17616	4100
47.25	11542	4750
48.1	9853	4840
48.7	8541	4900
50.75	6332	5300
52.75	6186	-
53.0	6408	-
54.4	6112	-
55.0	5848	-
56.0	6004	-
57.05	5933	-
58.4	5737	-
59.2	5878	-
61.2	5653	-
62.9	5700	-
72.2	5827	-

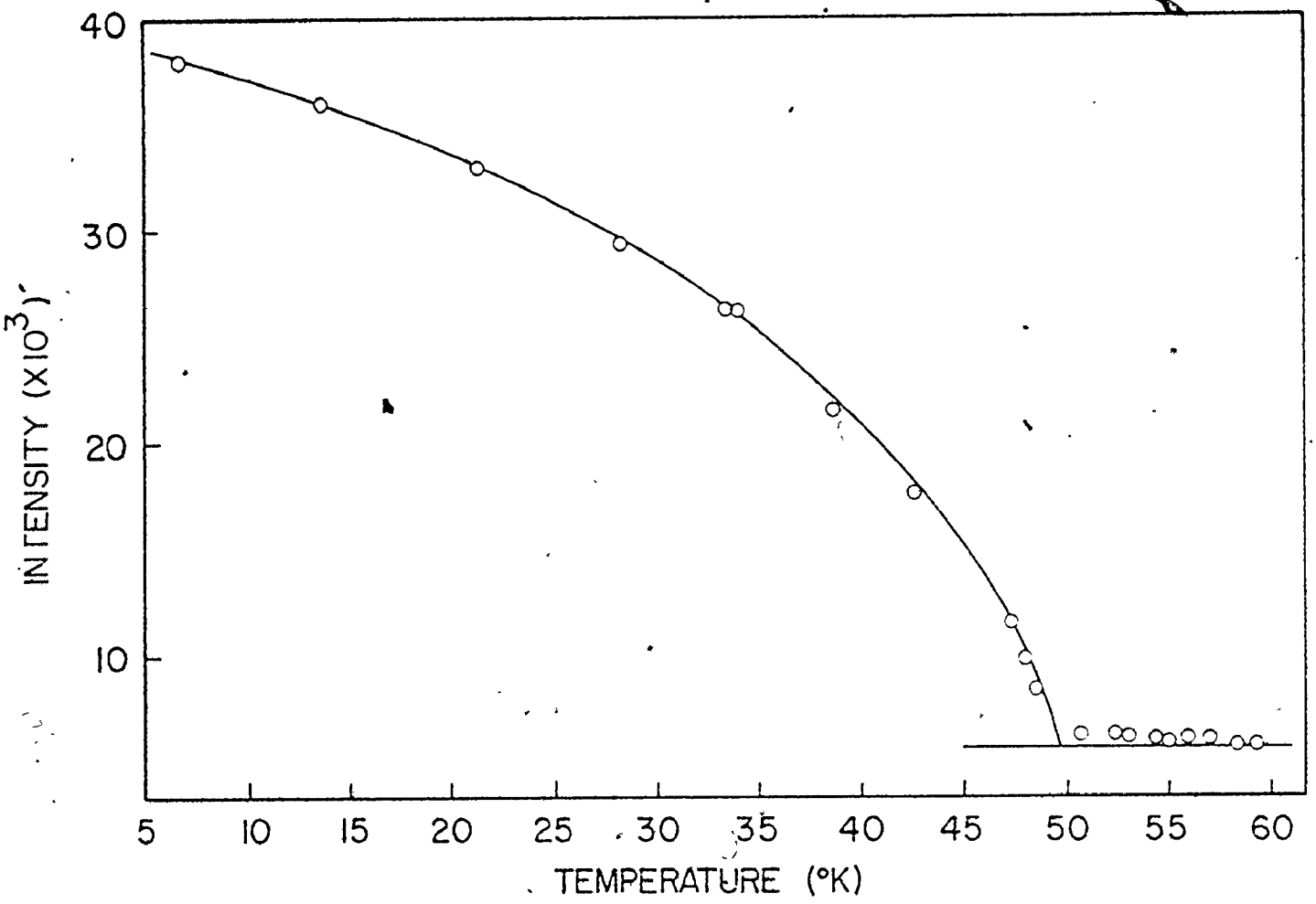

Fig. V-3 Temperature dependence of the superimposed magnetic peak intensity of (003) and (101) in $CsMnF_3$. The small circles are the observed data points and the solid curve is drawn by hand.

log plots of corrected peak intensity (I) versus reduced temperature $(1-T/T_c)$ for T_c = 49.8 K and 49.7 K, the points do not lie on a straight line. Far away from and close to T_c the points stay below the line. The opposite effect is observed for T_c = 49.5 K. The best graph corresponds to T_c = 49.6 K where most of the points, except for a few far away from T_c lie on the straight line (figure (V-4)). The points far away from T_c are insensitive to T_c. The value of critical exponent for T_c = 49.6 K is

$$\beta = 0.317 \pm .009 .$$

The error of 0.009 in β corresponds to a relative error of 0.1°K in temperature.

The critical index β has been measured for three other antiferromagnets. In $RbMnF_3$, Tucciarone et al (1971) find $\beta = 0.32 \pm .02$, in MnF_2, Heller (1966) finds $\beta = 0.335 \pm .005$ and in $KMnF_3$, Cooper et al (1966) find $\beta = 0.37$. No error was quoted in the last of these three measurements. It should perhaps also be mentioned that β for MnF_2 was measured by NMR technique and that this may not give a reliable result because the NMR frequency may not be proportional to M(T). Considering the errors involved, our result is in good agreement with the ones for $RbMnF_3$ and MnF_2 but it probably falls below the value for $KMnF_3$. We should mention that no theoretical method is known for determining β accurately for Heisenberg models, other than by application of the scaling

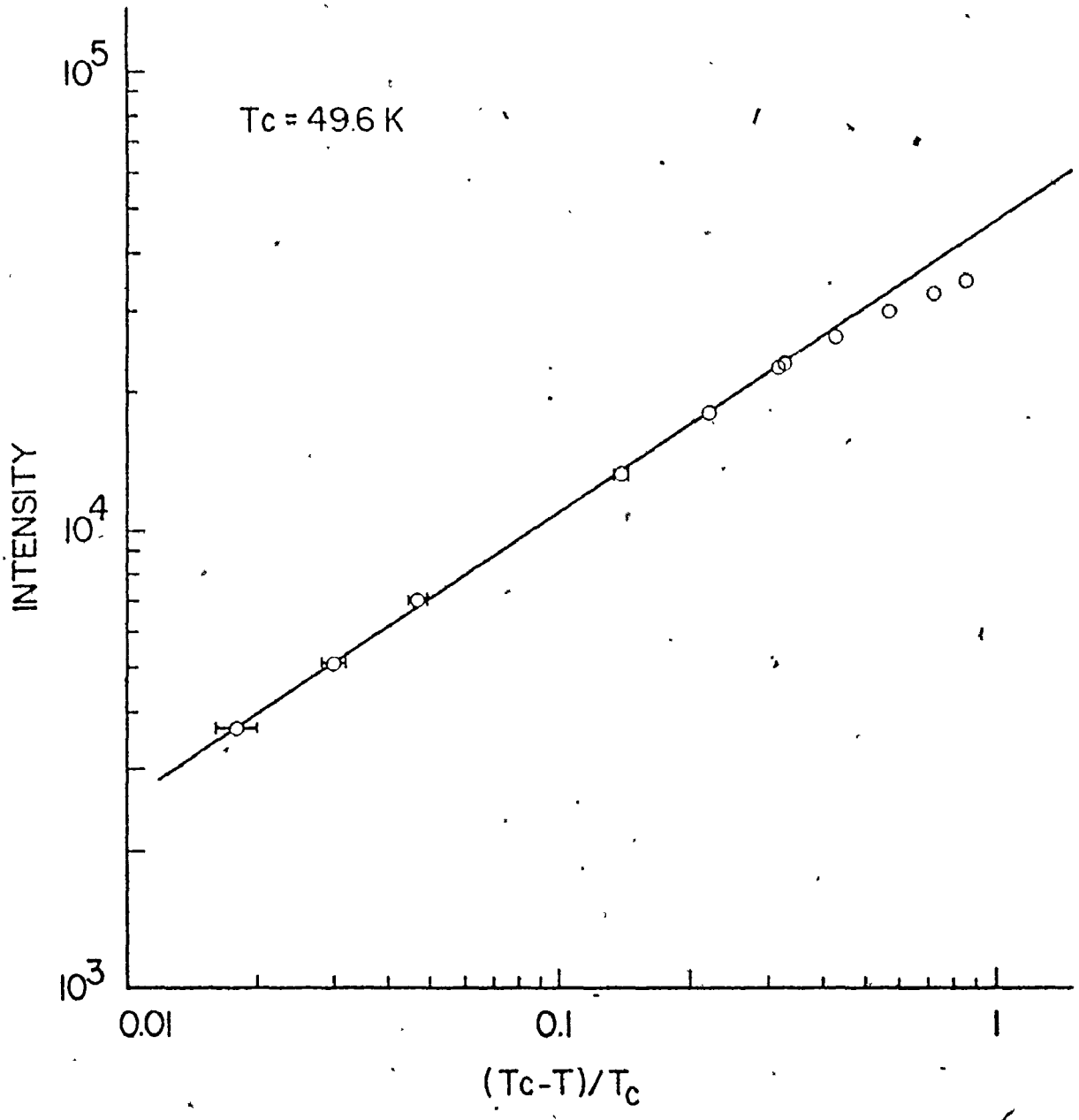

Fig. V-4 Log-log plot of the superimposed magnetic peak intensity of (003) and (101) in $CsMnF_3$ against $(T_c-T)/T_c$ for T_c = 49.6 K. The solid line has slope of 0.634.

law (Stanley 1971). The scaling law equation (Fisher 1967)

$$\beta = \Delta - \gamma \qquad \text{(V-3)}$$

can be used to predict β if the gap parameter 2Δ and the susceptibility exponent γ are known. γ and 2Δ have been estimated only for cubic lattices and two special cases of spin-$\frac{1}{2}$ and spin-infinity. Baker et al (1967) obtained $\gamma = 1.43 \pm .01$ and $2\Delta = 3.63 \pm .03$ for spin-$\frac{1}{2}$ Heisenberg model by high temperature expansion method. Then using equation (V-3) β was found to be $0.385 \pm .025$. For spin infinity Ferer et al (1971) found $\gamma = 1.405 \pm .02$ and $2\Delta = 3.54 \pm .03$. Using these values β comes up $0.364 \pm .03$. In both cases the experimental values fall below the values estimated by the scaling law.

The value of $T_c = 49.6$ K can be compared with $T_c = 53.5$ K and $T_c = 64$ K obtained by Lee et al (1963) and Pickart et al (1963) respectively. Since our thermometers were calibrated against a GaAs thermometer purchased from Scientic Instruments Inc. (section III-2), we can not be very sure about the absolute accuracy of $T_c = 49.6$ K. We believe that the value 64 K is definitely too high and the Néel temperature for $CsMnF_3$ should be in the region 47 K to 53 K.

CHAPTER VI

SUMMARY AND CONCLUSION

$CsMnF_3$ has hexagonal structure with a = 6.213±.003 Å and c = 15.074±.004 Å. The unit cell is built up of six closed-packed layers of Cs and F ions with Mn ions located in the fluorine octahedral holes between the layers. An interesting feature of this structure is that there are two different manganese sites. One third of the manganese atoms occupy the centers of those fluorine octahedra that share their corners with other octahedra, as in the perovskite structure, and the remaining two thirds of the manganese atoms are in distorted fluorine octahedra, that share one face and three corners with other octahedra.

In this thesis we have reported the results of our studies on two of the magnetic properties of this compound; the wave vector dependence of spin wave frequencies and the temperature dependence of magnetization.

Spin wave frequencies were measured along the two high symmetry directions (00ξ) and (ξ00) by inelastic neutron scattering techniques. In general the optic magnon peaks were weaker and broader than the acoustic magnon peaks. The observed magnon dispersion curves were smooth and were interpreted by spin wave theory.

To build up the theory we assumed a model with six magnetic sublattices per unit cell, two nearest neighbour exchange constants, J_{12} and J_{23}, and one second nearest neighbour exchange constant, J_{35}. We also assumed that the magnetic dipole-dipole interactions would be the main source of anisotropy.

We were able to obtain a stable configuration only when the spins were assumed to lie in the basal plane of the crystal. The best fit to the observed data was obtained when

$$J_{12} = 0.134 \pm .003 \text{ THz} \quad , \quad J_{23} = 0.094 \pm .0105 \text{ THz}$$

and

$$J_{35} = -0.0138 \pm .003 \text{ THz} .$$

The errors in the exchange constants correspond to two standard errors in the function F, which was minimized for the best fit. A model with only two nearest neighbour exchange constants, J_{12} and J_{23}, which was assumed by Seavey (1969), does not satisfy our observed results.

A similar effect to dipole-dipole interactions was found by assuming an effective anisotropy field of -2700±900 Oe along the crystal c axis. The direction of this effective field is in accord with the previous observations by K. Lee et al (1963), though the value 2700 Oe is much smaller than the value (7500 Oe) given by them. Our experimental results indicate clearly that 2700 Oe is the correct value for the anisotropy field.

No evidence was found to support the existence of a six-fold anisotropy energy in the crystal basal plane; if such a term exists (as is likely) it is much smaller than the term confining the spins to the basal plane.

The nature of the magnetic phase transition in $CsMnF_3$ was studied by measuring the magnetic peak intensity of the combined (10$\bar{1}$) plus (003) reflections over the temperature range of 6.8 K to 72.2 K. A powder sample was used to avoid extinction effects.

A sharp peak (indicative of magnetic long range order) is observed below T_c. The width (FHHW) of the peak stays constant throughout the temperature range and the peak position changes only by 0.1 degrees. The peak intensity decreases smoothly with temperature and the phase transition appears to have the typical properties of a second order phase transition.

The value for the critical exponent β was found to be

$$\beta = 0.317 \pm .009 \ .$$

The error in β corresponds to a relative error of 0.1°K in the temperature. This should be compared to the previous measurements in $RbMnF_3$, MnF_2 and $KMnF_3$ which are, respectively, $0.32 \pm .02$, $0.335 \pm .005$ and 0.37. For two special cases of the Heisenberg model, spin-$\frac{1}{2}$ and spin-infinity, the scaling

law predicts 0.385±.025 and 0.364±.03 respectively.

The Néel temperature was found to be 49.6 K, which can be compared to previous measurements of 53.5 K and 64 K. We can not be very sure about the absolute accuracy of our value, but we believe that it should be in the region 47 K to 53 K.

We hope these results will stimulate further theoretical and experimental work on more complex antiferromagnetic systems.

BIBLIOGRAPHY

Akhiezer, A.I., Bar'Yakhtar, V.G. and Peletminskii, S.V., "Spin Waves", North-Holland Publishing Co. (1968).

Anderson, P.W., Phys. Rev. 115, 2 (1959).

Bacon, G.E., "Neutron Diffraction", Oxford University Press (1962).

Baker, G.A. Jr., Gilbert, H.E., Eve, J. and Rushbrooke, G.S., Phys. Rev. 164, 800 (1967).

Belson, H.S. and Kriessman, C.J., Suppl. J. Appl. Phys. 30, 175 (1959).

Bloch, F., Z. Phys. 61, 206 (1930).

Bogoliubov, N. and Tyablikov, S., Zhur. Eksperim. Teor. Fiz. 19, 251 (1948).

Born, M. and Huang, K., "Dynamical Theory of Crystal Lattices", Oxford University Press (1954).

Brockhouse, B.N., Proceedings of the Symposium on Inelastic Scattering of Neutrons in Solids and Liquids, 113 (1961).

Brockhouse, B.N., Dewit, G.A., Hallman, E.D. and Rowe, J.M., Proceedings of the Symposium on Inelastic Scattering of Neutrons, 259 (1968).

Collins, M.F., Brit. J. Appl. Phys. 14, 805 (1963).

Cooper, M.J. and Nathans, R., J. Appl. Phys. 37, 1041 (1966).

Cooper, M.J. and Nathans, R., Acta Cryst. 23, 357 (1967).

Dirac, P.A.M., Proc. Roy. Soc. A123, 714 (1929).

Domb, C. and Green, M.S., "Phase Transitions and Critical Phenomena" (5 volumes), Academic Press (1972-1976).

Dyson, F.J., Phys. Rev. 162, 1217 (1956).

Egelstaff, P.A., "Thermal Neutron Scattering", Academic Press (1965).

Ferrer, M., Moor, M.A., and Wortis, M., Phys. Rev. B4, 3954 (1971).

Fisher, M.E., Rep. Phys. Prog. 30 (ii), 615 (1967).

Heisenberg, W., Z. Phys. 38, 411 (1926).

Heller, P., Phys. Rev. 146, 403 (1966).

Hennion, B. and Moussa, F., Ann. Phys. 233 (1972).

Holstein, F. and Primakoff, H., Phys. Rev. 58, 1908 (1940).

Keffer, F. and Loudon, R., J. Appl. Phys. Suppl. 32, 25 (1961).

Kramers, H.A., Physica 1, 182 (1934).

Kranendonk, J. van and Vleck, J.H. van, Rev.Mod.Phys. 1 (1958).

Krupica, S. and Sternberg, J., "Elements of Theoretical Magnetism", CRC Press (1968).

Landau, L.D. and Lifshitz, E.M., "Electrodynamics of continuous media", Pergamon Press (1960).

Larose, A., Ph.D. Thesis, McMaster University, Hamilton, Canada (1975).

Lee, K., Portis, A.M. and Witt, G.L., Phys. Rev. 132, 144 (1963).

Maleev, S.V., Sov. Phys.-JETP 6, 776 (1958).

Marshall, W. and Lovesey, S.W., "Theory of Thermal Neutron Scattering", Oxford University Press (1971).

Mattis, D.C., "The Theory of Magnetism", Harper and Rowe publishers (1965).

Nagai, O. and Yoshimori, A., Prog. Th. Phys. 25, 595 (1961).

Nagamiya, T., Yoshida, K. and Kubo, K., Advances in Physics 4, 1 (1955).

Néel, L., Ann. de Phys. 17, 64 (1932).

Pickart, S.J., Alperin, H.A. and Nathans, R., Inter. Coll. on Neutron Diffraction and Diffusion, Grenoble (1963).

Saunderson, D.H., Windsor, C.G., Evans, M.T. and Hutchison, E.A., IAEA Symp., Grenoble, 639 (1972).

Seavey, M.H., Phys. Rev. Lett. 23, 132 (1969).

Simanov, Y.P., Batsanova, L R. and Kovba, L.M., Zh. Neorgan. Khim 2, 2410 (1957).

Slater, J.C., Phys. Rev. 35, 509 (1930).

Smith, J. and Wijn, H.P., "Ferrites", John Wiley and Sons Inc., New York (1959).

Stanley, H.E., "Introduction to Phase Transitions and Critical Phenomena", Oxford University Press (1971).

Stoner, E.C., "Magnetism and Matter", Methuen and Co. Ltd. (1934).

Tondon, V.K., Ph.D. Thesis, McMaster University, Hamilton, Canada (1973).

Tucciarone, A., Lau, H.Y., Corliss, L.M., Delapalme, A. and Hastings, J.M., Phys. Rev. B4, 3206 (1971).

White, R.M., "Quantum Theory of Magnetism", McGraw Hill (1970).

Zalkin, A., Lee, K. and Templeton, D.H., J. Chem. Phys. 37,